Effect of Film-Hole Shape on Turbine Blade Film Cooling Performance

J.C. Han and S. Teng
Texas A&M University, College Station, Texas

February 2000

Since its founding, NASA has been dedicated to the advancement of aeronautics and space science. The NASA Scientific and Technical Information (STI) Program Office plays a key part in helping NASA maintain this important role.

The NASA STI Program Office is operated by Langley Research Center, the Lead Center for NASA's scientific and technical information. The NASA STI Program Office provides access to the NASA STI Database, the largest collection of aeronautical and space science STI in the world. The Program Office is also NASA's institutional mechanism for disseminating the results of its research and development activities. These results are published by NASA in the NASA STI Report Series, which includes the following report types:

- TECHNICAL PUBLICATION. Reports of completed research or a major significant phase of research that present the results of NASA programs and include extensive data or theoretical analysis. Includes compilations of significant scientific and technical data and information deemed to be of continuing reference value. NASA's counterpart of peer-reviewed formal professional papers but has less stringent limitations on manuscript length and extent of graphic presentations.

- TECHNICAL MEMORANDUM. Scientific and technical findings that are preliminary or of specialized interest, e.g., quick release reports, working papers, and bibliographies that contain minimal annotation. Does not contain extensive analysis.

- CONTRACTOR REPORT. Scientific and technical findings by NASA-sponsored contractors and grantees.

- CONFERENCE PUBLICATION. Collected papers from scientific and technical conferences, symposia, seminars, or other meetings sponsored or cosponsored by NASA.

- SPECIAL PUBLICATION. Scientific, technical, or historical information from NASA programs, projects, and missions, often concerned with subjects having substantial public interest.

- TECHNICAL TRANSLATION. English-language translations of foreign scientific and technical material pertinent to NASA's mission.

Specialized services that complement the STI Program Office's diverse offerings include creating custom thesauri, building customized data bases, organizing and publishing research results . . . even providing videos.

For more information about the NASA STI Program Office, see the following:

- Access the NASA STI Program Home Page at *http://www.sti.nasa.gov*

- E-mail your question via the Internet to help@sti.nasa.gov

- Fax your question to the NASA Access Help Desk at (301) 621-0134

- Telephone the NASA Access Help Desk at (301) 621-0390

- Write to:
  NASA Access Help Desk
  NASA Center for AeroSpace Information
  7121 Standard Drive
  Hanover, MD 21076

NASA/CR—2000-209932

Effect of Film-Hole Shape on Turbine Blade Film Cooling Performance

J.C. Han and S. Teng
Texas A&M University, College Station, Texas

National Aeronautics and
Space Administration

Glenn Research Center

February 2000

Available from

NASA Center for Aerospace Information
7121 Standard Drive
Hanover, MD 21076
Price Code: A04

National Technical Information Service
5285 Port Royal Road
Springfield, VA 22100
Price Code: A04

Table of Contents

NOMENCLATURE

C_x blade axial chord length (17cm)

d wake generator rod diameter

D film hole diameter

h local heat transfer coefficient

k thermal conductivity of blade material (0.159 W/m•°C)

k_{air} thermal conductivity of mainstream air

L film cooling hole length

M coolant-to-mainstream mass flux ratio or blowing ratio, $\rho_c V_c/\rho_m V$

n number of rods on wake generator

N speed of rotating rods

Nu local Nusselt number based on axial chord, hC_x/k_{air}

$\overline{Nu}$ spanwise-averaged Nusselt number

P film hole pitch

Re Reynolds number based on exit velocity and axial chord, $V_2 C_x/\nu$

S wake Strouhal number, $2\pi Ndn/(60V_1)$

SL streamwise length on the suction surface (33.1cm)

t liquid crystal color change time

T_c coolant temperature

T_f film temperature

T_i initial temperature of blade surface

T_m mainstream temperature

T_w liquid crystal color change from green to red

V local mainstream velocity along the blade suction surface at the film-hole location

V_c coolant hole exit velocity

V_1 cascade inlet velocity

V_2 cascade exit velocity

X streamwise distance from centerline of film cooling holes; streamwise distance from blade leading edge

Y perpendicular distance from blade surface

Z spanwise distance from centerline of film cooling holes

α	thermal diffusivity of blade material (0.135×10^{-6} m^2/s)
δ_2	local momentum thickness
η	local film cooling effectiveness
$\bar{\eta}$	spanwise-averaged film cooling effectiveness
ν	kinematic viscosity of cascade inlet mainstream air
θ	nondimensional coolant jet temperature $(T-T_m)/(T_c-T_m)$
ρ_c	coolant density
ρ_m	mainstream flow density

1.0 PROJECT SUMMARY

The detailed heat transfer coefficient and film cooling effectiveness distributions as well as the detailed coolant jet temperature profiles on the suction side of a gas turbine blade were measured using a transient liquid crystal image method and a traversing cold wire and a traversing thermocouple probe, respectively. The blade has only one row of film holes near the gill hole portion on the suction side of the blade. The hole geometries studied include standard cylindrical holes and holes with diffuser shaped exit portion (i.e. fanshaped holes and laidback fanshaped holes). Tests were performed on a five-blade linear cascade in a low-speed wind tunnel. The mainstream Reynolds number based on cascade exit velocity was 5.3×10^5. Upstream unsteady wakes were simulated using a spoke-wheel type wake generator. The wake Strouhal number was kept at 0 or 0.1. Coolant blowing ratio was varied from 0.4 to 1.2. Results show that both expanded holes have significantly improved thermal protection over the surface downstream of the ejection location, particularly at high blowing ratios. However, the expanded hole injections induce earlier boundary layer transition to turbulence and enhance heat transfer coefficients at the latter part of the blade suction surface. In general, the unsteady wake tends to reduce film cooling effectiveness.

2.0   INTRODUCTION

A continuing trend towards higher gas turbine inlet temperatures that are sufficient to melt airfoils and endwalls and have resulted in higher heat loads on turbine components. Hence, sophisticated cooling techniques must be employed to cool the components to maintain the performance requirements. Some turbine blades are cooled by ejecting cooler air from within the blade through discrete holes to provide a protective film on the surface exposed to the hot gas path. Cooling jet injection may result in higher heat transfer coefficients downstream of the injection location. However, the heat transfer rates can still be substantially reduced due to a decreased film-to-wall temperature difference. Many studies have presented heat transfer measurements on turbine blades with film cooling. Nirmalan and Hylton (1990), Abuaf et al. (1995), Ames (1997), and Drost and Bölcs (1998) studied film cooling heat transfer on film cooled turbine vanes. Camci and Arts (1990) and Takeishi et al. (1992) studied film cooling heat transfer on film cooled turbine blades. Ito et al. (1978), and Haas et al. (1992) studied the effect of coolant density on film cooling effectiveness on turbine blades.

The effect of unsteady wakes produced by upstream vane trailing edges has a strong effect on rotor blade surface heat transfer coefficient distributions. Several studies have focused on the effect of unsteady wakes on the downstream blade heat transfer coefficient distributions without film cooling. They all reported that unsteady wakes enhanced turbine blade heat transfer and caused earlier and longer laminar-turbulent boundary-layer transition on the suction surface. Few studies have focused on the effect of unsteady wakes on film cooled turbine blades. Abhari and Epstein (1994) conducted

heat transfer experiments on a film-cooled transonic turbine stage in a short duration turbine facility. They measured steady and time-resolved, chord-wise heat flux distributions at three spanwise locations. They concluded that film cooling reduces the time-averaged heat transfer by about 60% on the suction surface compared to the uncooled rotor blade. However, the effect is relatively low on the pressure surface. Ou et al. (1994), and Mehendale et al. (1994) simulated unsteady wake conditions over a linear turbine blade cascade with film cooling. They studied the effects of unsteady wake on a model turbine blade with multiple-row film cooling using air and CO_2 as coolants. They measured heat transfer coefficients and film cooling effectiveness at discrete locations using thin foil heating and multiple thermocouples. They concluded that heat transfer coefficients increase and film cooling effectiveness values decrease with an increase in unsteady wake strength. Du et al. (1998, 1999) used a transient liquid crystal technique to measure the detailed heat transfer coefficient and film effectiveness distributions over a film cooled turbine blade under the effect of upstream unsteady wakes. They concluded that unsteady wake slightly enhances Nusselt numbers but significantly reduces film cooling effectiveness on a film-cooled blade surface as compared to a film-cooled blade without unsteady wake. Teng et al. (1999) studied unsteady wake effect on film temperature and effectiveness distributions for a gas turbine blade with one row of cylindrical film holes near the suction side gill hole region. They concluded that unsteady wake reduces film cooling effectiveness. They also found out that film injection enhances the local heat transfer coefficient while the unsteady wake promotes earlier boundary-layer transition.

To improve the cooling effectiveness and thus increase the lifetime of gas turbine blades, an attempt has recently been made to contour the film hole geometry. Film cooling holes with a diffuser shaped expansion at the exit portion of the holes are believed to improve the film cooling performance on a gas turbine blade. The increased cross-sectional area at the hole exit compared to a standard cylindrical hole leads to reduction of the coolant velocity for a given blowing ratio. The momentum flux of the jet exiting the hole and the penetration of the jet into the mainstream will be reduced accordingly, which results in an increased cooling efficiency. Furthermore, lateral expansion of the hole provides an improved lateral spreading of the jet, which leads to a better coverage of the airfoil in the lateral direction and a higher laterally averaged film-cooling efficiency. A few previous studies have shown that expanding the exit of the cooling hole improves film-cooling performance in comparison to a cylindrical hole. Goldstein, et al. (1974) reported that overall improvements in adiabatic effectiveness were found for the flat plate film cooling with laterally expanded holes. Makki, et al. (1986) reported that the same improvements were found for forward expanded holes. Haller and Camus (1983) performed aerodynamic loss measurements on a 2-D transonic cascade. Holes with a spanwise flare angle of 25° were found to offer significant improvements in film-cooling effectiveness without any additional loss penalty. Schmidt, et al. (1994) and Sen, et al. (1994) compared a cylindrical hole to a forward expanded hole, both of them having compound angle injection for the flat plate film cooling. Although the spatially averaged effectiveness for the cylindrical and forward-expanded holes was the same, a larger lateral spreading of the forward expanded jet was found. Gritsch, et al. (1997, 1998) performed detailed measurements of the flat plate film

cooling effectiveness and heat transfer coefficients for holes with expanded exits. They reported that, compared to the cylindrical holes, both expanded holes show significantly improved thermal protection of the surface downstream of the ejection location, particularly at the high blowing ratios.

All of the above studies have proven that film cooling holes with a diffuser shaped expansion at the exit portion of the hole have improved film fooling performance in comparison to cylindrical holes. It is of great interest to understand the effect of the hole shape on blade film cooling performance under real turbomachinery flow conditions, i.e., consideration of the effect of surface curvature and pressure gradient that exists on a real turbine blade. However, most of the above mentioned shape hole film cooling studies are for flat plate geometry. There are very few studies present in open literature examining the effects of hole shape on turbine blade film cooling performance under steady and unsteady wake conditions. This study focuses on only one row of film holes near the suction-side gill hole portion in order to investigate the hole shape effect on the curved blade surface under strong flow acceleration conditions. Film cooling holes with and without exit expansions are studied and compared under steady and unsteady wake conditions. In the present study, a transient liquid crystal method is used to measure the detailed heat transfer coefficient and film effectiveness distributions, and a traversing cold wire and a traversing thermocouple probe to measure coolant jet temperature profiles of a gas turbine blade. The high resolution of the liquid crystal technique, combined with the coolant jet temperature profile measurement, provides a clear picture of how the heat transfer coefficient and film effectiveness distributions vary along the

5

blade surface with different film hole shapes. The results also provide a good database

for film cooling computational model development.

3.0 EXPERIMENTAL APPARATUS

Figure 1 (a) shows the schematic of the test section and camera locations. The test apparatus consists of a low speed wind tunnel with an inlet nozzle, a linear turbine blade cascade with the test blade in the center, and a suction type blower. The wind tunnel is designed to accommodate the 107.49° turn of the blade cascade. The cascade inlet mean velocity is about 20m/s. The mean velocity increases 2.5 times from the inlet of the cascade to the exit. The test apparatus was described in detail by Ou et al. (1994). A spoked wheel type wake generator, similar to the one used by Ou et al. (1994), simulated the upstream unsteady wake. The wake generator has 32 rods, each 0.63cm in diameter, to simulate the trailing edge of an upstream vane. The wake Strouhal number is adjusted by controlling the rod rotation speed (N). The error caused by using nonparallel rotating rods with a linear blade cascade was small and was discussed by Ou et al. (1994). The blade configuration, scaled up five times, produces a velocity distribution typical of an advanced high-pressure turbine blade row. The cascade has five blades, each with an axial chord length of 17cm and a radial span of 25.2cm. The blade spacing is 17.01cm at the cascade inlet and the throat-to-blade span ratio is 0.2. Du et al. (1998) presented the local-to-exit velocity ratio distribution around the blade as well as the instantaneous velocity, ensemble-averaged velocity and ensemble-averaged turbulence profiles at the cascade inlet under the effect of upstream unsteady wakes. The velocity on the suction side accelerates to about X/SL=0.5 (V/V_2=110%) and then decelerates slightly at the cascade exit. In the present study, a row of film holes is located near the suction side gill hole region, where V/V_2 is about 68%, the momentum thickness δ_2 is about 9×10^{-4}m and the momentum thickness Reynolds number is about

7

200 for steady flow. The unsteady wakes are actually velocity deficiencies caused by the blockage of mainstream flow by the rotating rods. The ensemble-averaged turbulence intensity profiles at the cascade inlet show that intensity could be as high as 20% inside the wake, but the time mean averaged turbulence intensity is about 10.4%. For cases without unsteady wake effect, the time mean averaged turbulence is about 0.7%.

The present film-cooled turbine blade model is the same as the one used by Teng et al. (1999). Figure 1 (b) presents a 2-D view of the film cooled turbine blade model. Its thermal conductivity is 0.159w/m•k and thermal diffusivity is 1.35×10^{-7} m^2/s. There is one cavity used to supply coolant to the row of film holes on the suction side. The film holes, 1.905mm in diameter and 10.16mm apart from one another (P/D=5.3), have a radial angle of 90° and a tangential angle of 40°. The film hole length is 15mm (L/D=7.9). The flow rate is controlled by a flowmeter. The coolant has been heated to about 110°F. The heated coolant flow is passed through a solenoid-controlled three-way diverter valve before the flow enters the coolant cavity inside the blade. The solenoid-controlled valve is connected to a switch that triggers the heated coolant flow into the cavity at the instant the transient test is initiated.

The film temperature profiles are measured at X/D=1, 5, 10, 15 from the centerline of the film cooling holes as shown in Figure 2. The measuring plane is perpendicular to the oncoming mainstream. The blade model is not heated and only the coolant is heated and ejected during the measurement of the film temperature profile. The coolant was heated to maintain a temperature difference from the free-stream at about 18°C. For cylindrical holes, the temperature field is measured using a cold-wire system (Teng et al., 1999). The cold-wire system includes a tungsten wire probe, 5μm in

diameter and 1.5mm in length, and a temperature bridge. The frequency response of the cold-wire is about 800Hz. For fanshaped and laidback fanshaped holes, the temperature field is measured using a traversing fine-gage thermocouple probe. The thermocouple bead size is about 0.004 inches and the probe size is about 0.01 inches. The response time of this fine gage thermocouple is 0.08sec.

The liquid crystal coated surface area is 7.2cm wide and the data acquisition area is 2.5cm wide along the midspan region of the test blade. In film cooling measurements, the test blade surface is heated uniformly using a heater box (Teng et al., 1999). The heater box has the blade shape and is slightly larger than the test blade. The insides of the heater box are instrumented with thin foil heaters and controlled by using several variacs to provide a near uniform surface temperature. The heater box is lowered to completely cover the test blade during heating. The heater box is raised completely to expose the test blade to the mainstream during the transient test. The blade surface temperature is monitored using embedded thermocouples during heating. The uniformity of surface temperature with heating is within ±1.2°C. An interpolation scheme was used to further reduce the temperature variation in the initial surface temperature to within ±0.2°C. In the present study, the blade surface is heated to a temperature above the liquid crystal blue color (37.2°C). The mainstream air is turned on by starting the suction-type blower. When the blower reaches the stable test flow conditions, the heater box is raised to expose the hot blade to the room temperature mainstream air within 0.1 seconds. When the heater box completely clears the blade height, the liquid crystal data acquisition system is automatically triggered. The liquid crystal color change time is measured using a high precision image processing system. Each of the transient tests lasts 60 to 90

seconds in average. The system consists of 2 cameras individually connected to a color frame grabber board in the PC and a monitor. Software is used to measure the time of color change of liquid crystals. During one test, only one camera is operational. Hence, we require 2 different runs with 2 different camera locations to measure one set of data on the suction side for a particular condition. Details on the image processing system were presented by Teng et al. (1999). The image processing system consists of an RGB camera, monitor and a PC with color frame grabber board.

Figure 3 presents the three types of hole geometries studied: cylindrical hole, fanshaped hole, and laidback fanshaped hole. The hole geometries are similar to those used by Gritsch et al. (1997). They have shown that, in flat plate geometry, expanded holes show significantly improved thermal protection of the surface downstream of the ejection location as compared to the cylindrical hole. In the present study, a row of 9 holes of each shape located near the blade suction side gill hole region has been employed. The diameter of the cylindrical hole (D) and diameter of the cylindrical inlet section of the expanded hole is1.91mm. For all geometries, the inclination angle is 40°, the pitch to diameter ratio is P/D=5.3, and the length to diameter ratio L/D is 7.9. The lateral expansion angle of both expanded holes is 7.24°. The exit forward expansion angle of the laidback fanshaped hole is 25°. For the fanshaped and laidback fanshaped hole, the calculation of the blowing ratio was based on the inlet cross-sectional area of these holes. In this study, this means that same blowing ratio provides same amount of coolant ejected under the same mainstream condition. Thus, the blowing ratio of the shaped holes can be directly compared to those of the cylindrical hole, which makes it more convenient to evaluate the effect of hole shape.

4.0   DATA ANALYSIS

A transient liquid crystal technique was used to measure the detailed heat transfer coefficients and film cooling effectiveness on the blade suction surface. The technique is similar to the one described by Teng et al. (1999). A one-dimensional transient conduction into a semi-infinite solid with convective boundary condition is assumed. The solution for surface temperature is obtained as

$$\frac{T_w - T_i}{T_m - T_i} = \left[1 - \exp(\frac{h^2 \alpha t}{k^2}) erfc(\frac{h\sqrt{\alpha t}}{k}) \right] \tag{1}$$

where T_w is the wall temperature when liquid crystals change to red from green (32.7°C) at time t, T_i is the initial surface temperature, T_m is the oncoming mainstream flow temperature, and α and k are the thermal diffusivity and conductivity of the blade material, respectively. The heat transfer coefficient is obtained from Equation (1). For film cooling tests, the mainstream temperature (T_m) in Equation (1) is replaced by the local film temperature (T_f), which is a mixture of the coolant (T_c) and mainstream temperatures. The film temperature is defined in terms of η, which is the film cooling effectiveness.

$$\eta = \frac{T_f - T_m}{T_c - T_m}; \quad \text{or} \quad T_f = \eta T_c + (1 - \eta) T_m \tag{2}$$

For the film cooling test, we obtain an equation similar to Equation (1)

$$\frac{T_w - T_i}{T_f - T_i} = \frac{T_w - T_i}{\eta T_c + (1 - \eta) T_m - T_i} = \left[1 - \exp(\frac{h^2 \alpha t}{k^2}) erfc(\frac{h\sqrt{\alpha t}}{k}) \right] \tag{3}$$

Two similar transient tests are run to obtain the heat transfer coefficient (h) and film cooling effectiveness (η). In the first test, the blade surface is heated and the coolant and the mainstream temperatures are nearly the same. In this case, there is only one

unknown, h, in the equation. For the second test, the coolant is heated to a temperature close to blade initial temperature. The calculated local heat transfer coefficient from the first test is substituted in the equation to obtain the local film cooling effectiveness. Each of the transient tests lasts about 60 to 90 seconds. The methodology is described in detail by Teng et al. (1999). The above equation is solved at each point on the blade surface (16,600 points) to obtain the detailed heat transfer coefficient and film cooling effectiveness distributions.

The average uncertainty in heat transfer coefficient measurement was estimated to be ±6.5%. The individual uncertainties in the measurement of the time of color change ($\Delta t = \pm 5\%$), the mainstream temperature ($\Delta T_m = \pm 1.3\%$), the initial temperature ($\Delta T_i = \pm 0.6\%$), the color change temperature ($\Delta T_w = \pm 3\%$), and the wall material properties ($\Delta \alpha / k^2 = \pm 2\%$) are included in the calculation of the overall uncertainty in the measurement. The uncertainty in the film cooling effectiveness measurement including the additional uncertainties in heat transfer coefficient measurement was estimated to be about 9.2%. The uncertainty in the immediate vicinity of the hole (less than 1 diameter around the hole) could be higher due to 2-D conduction effect.

A cold-wire and a thermocouple were used to measure the coolant jet temperature profiles on the blade suction side. The mean temperature fields are presented as a non-dimensional temperature defined similar to film effectiveness,

$$\theta = \frac{T - T_m}{T_c - T_m}; \qquad (4)$$

1200 data points were measured at each measurement plane at different X/D locations. At each data point, 36,864 samples were acquired and averaged to get time averaged and fluctuation temperatures. The uncertainty in the coolant jet temperature field

12

measurement was estimated to be 5.8% using cold-wire and less than 1% using thermocouple.

5.0   RESULTS AND DISCUSSION

Experiments were performed at a cascade exit Reynolds number of 5.3×10^5. The corresponding flow velocity at the cascade exit was 50m/s. Air as coolant was tested at blowing ratios of 0.4, 0.6, 0.8, and 1.2 for no rod no wake cases (S=0, $\overline{Tu}$=0.7%) and cases with wake (S=0.1, $\overline{Tu}$=10.4%). Since the film effectiveness distributions with the cylindrical hole have already been presented in Teng et al. (1999), here we focus on the film effectiveness distributions with the shaped holes.

1. Detailed Film Effectiveness Measurements

Figure 4 and Figure 5 presents the detailed film effectiveness distributions at different blowing ratios for fanshaped and laidback fanshaped holes, respectively. The level for η is from 0 to 0.2. Please note that in the jet center η has values up to 0.4.

Effect of Blowing Ratio. Since there are no film cooling hole at the leading edge of the blade model, the film streaks start where the row of film cooling holes (the only row of holes in this study) is located. Wider film steaks extend along the streamwise direction fairly straightly. The streaks are gradually weakened as they extend further away from the film cooling holes. For the cases without unsteady wake effects (S=0), the film effectiveness of the fanshaped holes (Figure 4a) decreases at first with the increase of blowing ratio. The film streaks are observable from X/D=0 to 20 for a blowing ratio of M=0.4. The observable streaks reduce considerably as the blowing ratio increases to M=0.6. For the case of M=0.8, the film streaks become even shorter but wider. The film coverage area increases again as the blowing ratio increases further to M=1.2. The case

of M=1.2 provides the best thermal protection over the blade surface compared to all the other three lower blowing ratios. For the laidback fanshaped holes (Figure 5a), the film coverage area increases with the increase of blowing ratio over the blade surface. Compared with fanshaped holes, the blowing ratio has a monotonic effect on the film protection area for laidback fanshaped holes: the film coolant trace is barely seen for low blowing ratio of M=0.4, while the highest blowing ratio case of M=1.2 produces downstream of the film cooling holes a coolant trace which is even stronger than that produced by fanshaped holes.

Effect of Unsteady Wake. For fanshaped holes with unsteady wake effects (Figure 4b), the coolant jet dilutes faster into the mainstream and the film protection in the front area decreases for cases with lower blowing ratios (M=0.4 and 0.6) than the cases without wake effects. Only a small front portion (X/D<10) of the suction surface is covered by the film cooling jet. However, with unsteady wake effect, film coverage in the front area increases for cases of higher blowing ratios (M=0.8 and 1.2). For laidback fanshaped holes (Figure 5b), unsteady wake has reduced film effectiveness for all blowing ratios.

All this indicates that unsteady wake has a strong effect on the film cooling protection area. Generally, addition of unsteady wake results in lower film cooling effectiveness at the area downstream of film hole due to the intensive mixing between mainstream and coolant jet, except for the case of high blowing ratio near fanshaped holes.

2. Spanwise-averaged Film Effectiveness Distributions

Figure 6 and Figure 7 present the spanwise-averaged film effectiveness distribution for fanshaped and laidback fanshaped holes.

Effect of Blowing Ratio. For cases without unsteady wake effect (Figure 6a, 7a), it is observed that, for all blowing ratio cases, spanwise-averaged film effectiveness decreases all the way from X/D=0 to 25. For fanshaped holes (Figure 6a), the spanwise-averaged film effectiveness decreases with the increase of blowing ratio but increases again when blowing ratio increases to 1.2. For laidback fanshaped holes (Figure 7a), spanwise-averaged film effectiveness increases with the increase of blowing ratio over the whole surface. Blowing ratio M=1.2 produces the highest spanwise-averaged film effectiveness for both the fanshaped and laidback fanshaped holes.

Effect of Unsteady Wake. For fanshaped holes (Figure 6b), the addition of unsteady wake effect has made the spanwise-averaged film effectiveness decrease for lower blowing ratios of M=0.4 and 0.6. For higher blowing ratios of M=0.8 and 1.2, the spanwise-averaged film effectiveness increases from X/D=0 to 25. For laidback fanshaped holes (Figure 7b), the unsteady wake effect makes the spanwise-averaged film effectiveness decrease for all blowing ratios.

Effect of Hole Shape. Figure 8 compares the spanwise-averaged film effectiveness distributions of fanshaped and laidback fanshaped holes with that of standard cylindrical holes (Teng et al. 1999) for X/D up to 25 downstream of film hole. For cases without unsteady wake effect (Figure 8a) with a high blowing ratio of M=1.2, the spanwise-averaged film effectiveness of laidback fanshaped holes is slightly higher than that of fanshaped holes but much higher than that of cylindrical holes. For cases without unsteady wake effect with a low blowing ratio of M=0.6, the spanwise-averaged

film effectiveness of fanshaped holes is slightly higher than that of laidback fanshaped holes but much higher than that of cylindrical holes. For cases with unsteady wake effect (Figure 8b), the spanwise-averaged film effectiveness of fanshaped holes is higher than that of laidback fanshaped holes and subsequently much higher than that of cylindrical holes for both low and high blowing ratios. This concludes that both fanshaped and laidback fanshaped holes have much better thermal protection than cylindrical holes under both steady and unsteady flow conditions. Particularly, fanshaped holes provide the best thermal protection for all blowing ratios under unsteady flow conditions.

3. Detailed Heat Transfer Coefficient Measurements

Figures 9, 10, and 11 present the detailed heat transfer coefficient distributions for cylindrical, fanshaped and laidback fanshaped cooling holes, respectively. Figures (a1) through (a5) are for the cases without wake effect and Figures (b1) through (b5) are for the cases with wake effect. Additionally, (a1) and (b1) are for the cases without film-holes and the others in each group have blowing ratios ranging from 0.4 to 1.2.

For a no film-hole blade without wake effect case (a1), the Nusselt numbers drop rapidly from the leading edge to about X/SL=0.5 on the suction surface, and then increase again due to the boundary-layer transition to turbulent flow. The Nusselt numbers also decrease along the streamwise direction for a no film-hole blade with wake effect (case b1) but the boundary layer transition occurs much earlier (X/SL=0.25) for this case than for case a1. Also, the Nusselt numbers for case (b1) are higher than case (a1) before the transition begins.

Film injection through cylindrical holes (Figure 9) causes the Nusselt numbers at locations right behind the film holes to increase significantly due to the mainstream and coolant jet interaction. Traces of high Nusselt numbers are formed right behind the film holes. The higher the blowing ratio, i.e., the more mixing between the mainstream and the coolant jet, the longer this trace of highly-increased Nusselt numbers. The film injection disturbs the boundary layer, which causes transition to occur slightly earlier for cases (a2) through (a4) than case (a1). As soon as the boundary layer transition begins, the Nusselt numbers increase at about the same rate as case (a1), and keep increasing further down the blade before beginning to decrease. The same is true for the cases with both film cooling and unsteady wake effect, as seen by comparing cases (b2) through (b4) with case (b1). However, notice that, with or without film cooling, the addition of unsteady wake has caused the boundary layer transition to occur significantly earlier than the cases without unsteady wake. This is because unsteady wake interacts with the boundary layer; thus causing an earlier boundary layer transition and enhancing the surface heat transfer. Also, the cases with wake effect show that streaks of high Nusselt numbers right after the film holes are a little shorter when compared to the cases without wake effect. This is due to the unsteady wake, which causes the cooling jet to dilute faster along the streamwise direction than in the cases without unsteady wake.

For film injection through fanshaped holes (Figure 10), the Nusselt numbers right behind the film ejection location are significantly reduced when compared with the no film-hole case (a1). Traces of low Nusselt number are formed right behind the fanshaped film holes. This is because film injection through the fanshaped holes has a lower momentum compared with a cylindrical hole case with the same blowing ratio. The

18

lower momentum coolant jets from the fanshaped holes tend to stay closer to the blade surface, which reduces interaction (mixing) with the mainstream. Nusselt numbers behind the injection location increase along the streamwise direction as the mainstream begins to interact with the coolant jet. The Nusselt numbers also increase with the increase of blowing ratio due to the increased jet-to-mainstream interaction. Similar to the cylindrical hole cases, the boundary-layer transition for fanshaped holes (a2) through (a5) occurs slightly earlier than the no film-hole case (a1) because of the film injection. As soon as the boundary layer transition begins, the Nusselt numbers increase at a slower rate than the no film-hole case (a1), and keep increasing further down the blade before beginning decrease again. The same is true for cases with both film cooling and unsteady wake effect, as seen by comparing cases (b2) through (b4) with case (b1). The addition of the unsteady wake effect causes boundary layer transition to occur significantly earlier than in the cases without unsteady wake. Also, for cases with wake effect, the streaks of low Nusselt region right after the film holes are reduced compared with cases without wake effect, which is due to the interaction between the unsteady wake and the boundary layer.

Traces of low Nusselt number form right behind the film holes for cases of laidback fanshaped holes (Figure 11). The Nusselt numbers are slightly higher and the boundary layer transition occurs slightly earlier in comparison with their corresponding cases for fanshaped holes. The wide traces of low-Nusselt number right behind the fanshaped and laidback fanshaped film holes, especially for the cases without wake effect, indicate a low heat transfer rate between the blade surface and the cooling jet, and thus a much improved thermal protection in comparison to the standard cylindrical hole

19

film cooling. However, film injection through fanshaped and laidback fanshaped holes induce earlier boundary layer transition compared with cylindrical holes. The Nusselt number after boundary layer transition is also higher for fanshaped and laidback fanshaped hole injection.

4. Spanwise-Averaged Heat Transfer Coefficient Distributions

Figure 12, 13, and 14 present the spanwise-averaged Nusselt number distributions of cylindrical, fanshaped and laidback fanshaped holes for (a) steady flow and (b) unsteady flow with wake effect. The small arrows on the horizontal coordinate indicate the location of film injection. The results for the no film-hole blade with and without wake effect agree with those for the same cases from Ou et al., who used the thin-foil-thermocouple technique to study the heat transfer coefficient over the same turbine blade model.

Figure 12 presents the spanwise-averaged Nusselt number distributions for film injection through cylindrical holes. The spanwise-averaged Nusselt number shows a peak increase right downstream of the jet ejection location. It then decreases along the streamwise direction until it reaches the boundary layer transition location, where it begins to increase again to reach its second peak value. The second peak value is higher than the first one. For the cases with wake effect, however, the spanwise-averaged Nusselt numbers don't drop as low as the cases without wake effect before they begin to increase again due to a much earlier boundary-layer transition. Figure 12 shows that the Nusselt numbers downstream of the injection location increase with blowing ratio. This is because an increased blowing ratio causes more interaction (mixing) between the

coolant jet and the mainstream and, thus, increase the heat transfer coefficients. For a high blowing ratio of 1.2, the Nusselt numbers downstream of the injection location can increase up to 60 percent. The spanwise-averaged Nusselt numbers do not show much difference between different blowing ratios after the boundary layer transition. The addition of the unsteady wake effect promotes earlier boundary layer transition for all blowing ratios. In comparison to cases without wake effect, the spanwise-averaged Nusselt numbers do not drop much before the boundary layer transition occurs. The blowing ratio effect is very small compared with the effect of unsteady wake as far as the boundary-layer transition location is concerned.

Figure 13 shows that the spanwise-averaged Nusselt numbers also increase with the increase of blowing ratio for film injection through fanshaped holes. However, the spanwise-averaged Nusselt numbers right behind the film ejection location are lower than that of the no film-hole case. The Nusselt numbers downstream of the injection location can decrease up to 40 percent for a low blowing ratio of 0.4. Boundary layer transition occurs earlier as the blowing ratio increases. With the addition of unsteady wake, boundary layer transition occurs even earlier, but distinguishes the blowing ratio effect on boundary layer transition.

Film injection through laidback fanshaped holes (Figure 14) has spanwise-averaged Nusselt number distributions that are insensitive to blowing ratios, either under steady or unsteady flow conditions. At the locations right after the film injection, the spanwise-averaged Nusselt numbers are slightly lower than that of no film-hole case when there is no wake effect, while they are much lower (up to 30 percent) than when

there is wake effect.   Unsteady wake effect also promotes earlier boundary transition for film injection through laidback fanshaped holes.

Figure 15 presents the effect of hole shape on spanwise-averaged Nusselt number distributions for cases at a low blowing ratio of M=0.6. For film injection through fanshaped and laidback fanshaped holes, the spanwise-averaged Nusselt numbers right after the film ejection location are much lower than that for the cylindrical hole case. This implies that, for fanshaped and laidback fanshaped hole injection, the coolant jet with reduced momentum tends to attach to the blade surface and thus reduces the interaction with mainstream at locations right after the film injection. However, the low momentum jet may stay in but disturb the laminar boundary layer along the blade surface This causes an earlier boundary layer transition for both fanshaped hole injections in comparison with the cylindrical hole injection. Due to earlier boundary layer transition, the spanwise-averaged Nusselt numbers of both fanshaped and laidback fanshaped holes are much higher than that of the cylindrical hole case in the latter part of the blade surface.   The addition of unsteady wake has led to an increased Nusselt number difference in the front part of the blade surface: the region downstream of injection where the spanwise-averaged Nusselt numbers of fanshaped and laidback fanshaped holes are less than that of the cylindrical hole case is more than doubled in the streamwise direction.   However, the boundary layer transition location is almost the same for the three types of film hole injection and the no film-hole case when there is unsteady wake effect.

Figure 16 presents the effect of hole shape on spanwise-averaged Nusselt number distributions for cases with a high blowing ratio of M=1.2. The general trend is almost

the same as the cases with M=0.6. For the cases under steady flow condition, the spanwise-averaged Nusselt number is higher than that of no film-hole case for all three kinds of holes. Film injection through cylindrical holes produce the highest spanwise-averaged Nusselt numbers in the region right after the film injection location, while fanshaped and laidback fanshaped hole injection have higher spanwise-averaged Nusselt numbers at the latter part of the blade surface. With the addition of unsteady wake, the hole effect is intensified at the front part of the blade. In the region right after film injection, the spanwise-averaged Nusselt numbers for fanshaped and laidback fanshaped hole injection are much lower than that of cylindrical hole injection. The differences of the spanwise-averaged Nusselt numbers for different hole injection are reduced at the rear part of the blade surface. The boundary layer transition location is almost the same for the three types of film hole and the no film-hole case when there is unsteady wake effect.

5. Coolant Jet Temperature Field Measurements

A traversing cold wire was used to measure the coolant jet temperature profiles of cylindrical cooling holes, while a traversing thermocouple was used to measure the coolant jet temperature profiles of fanshaped and laidback fanshaped cooling holes. Due to the delicacy of the cold wire, we could not approach very close to the blade wall surface (in the Y direction). In the following figures there is no data at the near wall portion for cylindrical holes, while complete data planes were obtained for fanshaped and laidback fanshaped holes. This is because we could approach thermocouple until it touched the blade surface. However, we can see from the figures that the incomplete data planes for the cylindrical holes supplied us with enough information to understand the

behavior of the cooling jet coming out of the cylindrical holes. The level for θ is from 0 to 0.2 with regard to η. Please note that in the jet center θ has values up to 0.45.

Figure 17 presents the coolant jet temperature contours for cylindrical, fanshaped, and laidback fanshaped holes at X/D=5 and 10 with a blowing ratio of M=1.2 under steady flow conditions. The coolant jet coming out of the cylindrical hole maintains an elliptic shape, with the central part of the heated coolant jet having the highest mean temperature. The film coverage area is very narrow in the spanwise direction (small Z/P) but long in the boundary layer direction (large Y/D). With the blowing ratio as high as 1.2, the coolant jet almost lifts off into the mainstream, with only a small part of the jet periphery touching the blade surface, thus providing poor thermal protection. As it moves farther down the streamwise direction (from X/D=5 to X/D=10), the coolant jet is gradually mixed with and entrained into the mainstream. The jet temperature decreases substantially and there is barely any thermal protection over the blade surface at X/D=10. On the other hand, the coolant jets coming out of fanshaped and laidback fanshaped holes show profiles in the shape of a half-circle. The central part of the jet with the highest mean temperature touches the blade surface, thus provides good coolant protection over the blade surface. Since the coolant jets are attached closely to the blade surface, the mixing between the jets and the mainstream is not strong. The coolant jets are still in good shape and provide good protection over the blade surface at X/D=10.

Effect of Blowing Ratio. Figure 18 presents detailed film temperature profiles for the cylindrical, fanshaped, and laidback fanshaped holes for steady flow (S=0) at a blowing ratio of M=1.2. Compared with the cylindrical cooling holes, both the

fanshaped and laidback fanshaped holes provide much better and wider coolant protection over the blade spanwise surface (Z/P). The momentum flux of the jet exiting the hole and the penetration of the jet into the mainstream is reduced. The coolant jet is attached close to the surface and also spreading out along the spanwise direction, i.e., there is increased coverage in the Z/P direction but reduced jet penetration into the mainstream in the Y/D direction. Actually, the film jets coming out of the adjacent fanshaped holes expands so widely in the spanwise direction that their peripheries almost merge with each other, thus providing an almost continuous protection (greater Z/P) over the whole blade surface. The film cooling behavior of laidback fanshaped holes is not found to be better than that of fanshaped holes in the film temperature field measurement. Due to too much hole expansion in both the spanwise and streamwise directions, the laidback fanshaped holes have reduced coolant protection in the spanwise direction, i.e., reduced Z/P coverage, but increased jet penetration into the mainstream in the Y/D direction compared with the fanshaped holes.

Figure 19 presents the detailed film temperature profiles for the cylindrical, fanshaped, and laidback fanshaped holes for steady flow (S=0) at a blowing ratio of M=0.8. For cylindrical holes, the film temperature profiles shrink considerably in comparison to cases with a blowing ratio of M=1.2. The coolant jet has a better attachment to the blade surface at M=0.8. This is because the jet momentum decreases with a decreased blowing ratio. The penetration of the jet into the mainstream is not so strong and tends to attach to the blade surface. The mixing process between the jet and the mainstream is slowed, also, and the coolant jet still retains a large center area of high temperature even when X/D reaches 10. For fanshaped and laidback fanshaped holes, the

25

film temperature profiles are also reduced. The jet penetration into the mainstream in the Y/D direction is greatly reduced for fanshaped holes. However, there is still large coolant coverage in the Z/P direction for both the fanshaped and laidback fanshaped holes. They still provide much better coolant protection over the blade surface.

Effect of Unsteady Wake. Figure 20 presents the detailed film temperature profiles for the three kinds of film hole shapes at a blowing ratio of M=1.2 and under unsteady flow conditions (S=0.1). Film coolant jets, for cases with unsteady wake effect, dilute faster in comparison with their corresponding cases without wake effect (Figure 15). Unsteady wake has a greater effect on the film temperature field of cylindrical holes than that of fanshaped and laidback fanshaped holes. This is because the film jet coming out of the cylindrical holes lifts off into the mainstream flow, resulting in a larger contacting area with the unsteady mainstream (large Y/D) as well as more intensive mixing between the unsteady mainstream and the coolant jet. Film jets coming out of fanshaped and laidback fanshaped holes tend to attach close to the blade surface. They come into contact largely within the boundary layer (within the smaller Y/D) and the mixing between the unsteady mainstream and the coolant jet is not as strong as the cylindrical hole case.

Figure 21 presents the detailed film temperature profiles at a blowing ratio of M=0.8 and under unsteady flow conditions (S=0.1). Again, with unsteady wake, coolant jet dilutes faster into the mainstream in comparison with corresponding cases without wake effect (Figure 16). Unsteady wake has a greater effect on the film temperature field of cylindrical holes than that of fanshaped and laidback fanshaped holes.

26

6.0 CONCLUSIONS

I. Conclusions on the Effect of Film-hole Shape on Turbine Blade Film Effectiveness Distribution

1. For the blowing ratio range used in this study, fanshaped and laidback fanshaped holes provide better film cooling effectiveness for both steady flow and unsteady flow with wake effects. The spanwise-averaged film effectiveness of fanshaped and laidback fanshaped holes can be up to two times of that of cylindrical holes.

2. In general, fanshaped holes provide better film cooling effectiveness than laidback fanshaped holes, and subsequently much better than cylindrical holes.

3. For cylindrical holes, film cooling effectiveness decreases as the blowing ratio increases form 0.6 to 1.2. However, for fanshaped and laidback fanshaped holes, film cooling effectiveness increases as the blowing ratio increases form 0.6 to 1.2.

4. Unsteady wake tends to decrease film cooling effectiveness, except for the higher blowing ratio cases (M=0.8 and 1.2) from X/D=0 to 25 of fanshaped holes, where the film cooling effectiveness increases.

5. The film effectiveness distribution measured with the liquid crystal technique provides the detailed information about the variation of film effectiveness along both the streamwise and the spanwise direction, while the coolant jet temperature profiles measured with the thermocouple probe help to explain and confirm the fact that fanshaped and laidback fanshaped holes have better film cooling performance than cylindrical holes.

II. Conclusions on the Effect of Film-hole Shape on Turbine Blade Heat Transfer Coefficient Distribution

1. For film injection through cylindrical holes, the Nusselt numbers at the downstream of the injection location increase with an increase in blowing ratio. The Nusselt numbers downstream of the injection location can increase up to 60 percent for a high blowing ratio of 1.2. Unsteady wake promotes earlier boundary layer transition regardless of the blowing ratio effect.

2. For film injection through fanshaped holes, the Nusselt numbers downstream of the injection location increase with an increase in blowing ratio; however, they are lower than that of the no film-hole case. The Nusselt numbers downstream of the injection location can decrease up to 40 percent for a low blowing ratio of 0.4. However, fanshaped hole injection promotes earlier boundary layer transition as the blowing ratio increases. Unsteady wake causes earlier boundary layer transition regardless of the blowing ratio effect.

3. The Nusselt numbers are insensitive to blowing ratios for film injection through laidback fanshaped holes. Again, unsteady wake causes an even earlier boundary layer transition regardless of the blowing ratio effect.

4. For steady flow, when compared with cylindrical holes, both fanshaped and laidback fanshaped holes have much lower Nusselt numbers right after the film injection location. However, they cause higher heat transfer coefficients in the latter part of the blade surface due to earlier boundary layer transition.

5. For unsteady flow, when compared with cylindrical holes, both fanshaped and laidback fanshaped holes also have much lower Nusselt numbers right after the film injection location. They have almost the same boundary layer transition location as the cylindrical hole case, yet their Nusselt numbers are higher after transition into the turbulent region.

III. Conclusions on the Effect of Film-hole Shape on Turbine Blade Film Coolant Jet Temperature Profile Development

Detailed measurements of film coolant jet temperature profile on a gas turbine blade have been implemented. The film cooling hole geometries studied include standard cylindrical holes and holes with diffuser shaped exit region (i.e. fanshaped holes and laidback fanshaped holes). Results show that the cooling hole shape has an important impact on film coolant jet temperature profile development. Both kinds of expanded holes have significantly improved the thermal protection of the surface downstream of the ejection location, particularly at high blowing ratios, for both steady and unsteady flow conditions.

7.0 REFERENCES

Abhari, R. S., and Epstein, A. H., 1994, "An Experimental Study of Film Cooling in a Rotating Transonic Turbine," *ASME Journal of Turbomachinery*, Vol. 116, pp. 63-70.

Abuaf, N., Bunker, R., and Lee, C. P., 1995, "Heat Transfer and Film Cooling Effectiveness in A Linear Airfoil Cascade," ASME paper 95-GT-3.

Ames, F. E., 1997, "Aspects of Vane Film Cooling with High Turbulence: part I - Heat Transfer, part II - Adiabatic Effectiveness," ASME paper 97-GT-239, 97-GT-240.

Camci, C., and Arts, T., 1990, "An Experimental Convective Heat Transfer Investigation Around a Film-Cooled Gas Turbine Blade," *ASME Journal of Turbomachinery*, Vol. 112, pp. 497-503.

Drost, U., and Bölcs, A., 1998, "Investigation of Detailed Film Cooling Effectiveness and Heat Transfer Distributions on A Gas Turbine Airfoil," ASME paper 98-GT-20.

Du, H., Han, J. C., and Ekkard, S. V., 1998, "Effect of Unsteady Wake on Detailed Heat Transfer Coefficient and Film Effectiveness Distributions for A Gas Turbine Blade," *ASME Journal of Turbomachinery*, Vol. 120, pp. 808-817.

Du, H., Ekkad, S. V., and Han, J. C., 1999, "Effect of Unsteady Wake with Trailing Edge Coolant Ejection on Film Cooling Performance for A Gas Turbine Blade," *ASME Journal of Turbomachinery*, Vol. 121, pp. 448-455.

Goldstein, R., Eckert, E., and Burggraf, F., 1974, "Effects of Hole Geometry and Density on Three-Dimensional Film Cooling," *Int. J. Heat Mass Transfer*, Vol. 17, pp. 595-607.

Gritsch, M., Schulz, A., and Wittig, S., 1997, "Adiabatic Wall Effectiveness Measurements of Film-Cooling Holes with Expanded Exits," ASME Paper 97-GT-164.

Gritsch, M., Schulz, A., and Wittig, S., 1998, "Heat Transfer Coefficient Measurements of Film-Cooling Holes with Expanded Exits," ASME Paper 98-GT-28.

Haas, W., Rodi, W., and Schönung, B., 1992, "The Influence of Density Difference Between Hot and Coolant Gas on Film Cooling by a Row of Holes: Predictions and Experiments," *ASME Journal of Turbomachinery*, Vol. 114, pp. 747-755.

Haller, B. And Camus, J., 1983, "Aerodynamic Loss Penalty Produced by Film Cooling Transonic Turbine Blades," ASME Paper 83-GT-77.

Ito, S., Goldstein, R. J., and Eckert, E. R. G., 1978, "Film Cooling of a Gas Turbine Blade," *ASME Journal of Engineering for Power*, Vol. 100, pp. 476-481.

Kohli, A. and Bogard, D. G., 1998, "Fluctuating Thermal Field in the Near-Hole Region for Film Cooling Flows," *ASME Journal of Turbomachinery*, Vol.120, pp. 86-91.

Makki, Y. And Jekubowski, 1986, "An Experimental Study of Film Cooling from Diffused Trapezoidal Shaped Holes," AIAA Paper 86-1326.

· Mehandale, A. B., Han, J. C., Ou, S., and Lee, C. P., 1994, "Unsteady Wake Over a Linear Turbine Blade Cascade with Air and CO_2 Film Injection: Part II - Effect on Film Effectiveness and Heat Transfer Distributions," *ASME Journal of Turbomachinery*, Vol. 116, pp. 730-737.

Nirmalan, V., and Hylton, L., 1990, "An Experimental Study of Turbine Vane Heat Transfer with Leading Edge and Downstream Film Cooling," *ASME Journal of Turbomachinery*, Vol. 112, pp. 477-487.

Ou, S., Han, J. C., Mehendale, A. G., and Lee, C. P., 1994, "Unsteady Wake Over a Linear Turbine Blade Cascade with air and CO_2 Film Injection: Part I - Effect on Heat Transfer Coefficients," *ASME Journal of Turbomachinery*, Vol.116, pp. 721-729.

Schmidt, D., Sen, B., and Bogard, D., 1994, "Film Cooling with Compound Angle Holes: Adiabatic Effectiveness," ASME Paper 94-GT-312.

Sen, B., Schmidt, D. L., and Bogard, D. G., 1994, "Film Cooling with Compound Angle Holes: Heat Transfer," ASME Paper 94-GT-311.

Takeishi, K., Aoki, A., Sato, T., and Tsukagoshi, K., 1992, "Film Cooling on a Gas Turbine Rotor Blade," *ASME Journal of Turbomachinery*, Vol. 114, pp. 828-834.

Teng, S., Sohn, D. K., and Han, J. C., 1999, "Unsteady Wake Effect on Film Temperature and Effectiveness Distributions for A Gas Turbine Blade," ASME Paper 99-GT-172.

8.0   Figures 1–21

RGB Camera

Mainstream

RGB Camera

Wake Generator

mainstream

Mainstream

Film coolant jet

40°

1.9mm

Coolant supply channel

25.4mm

X/SL=0.12

1.9mm

9.5mm

Impingement channel
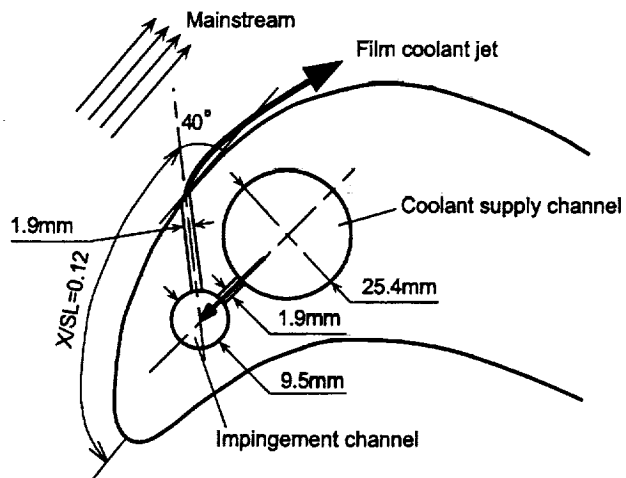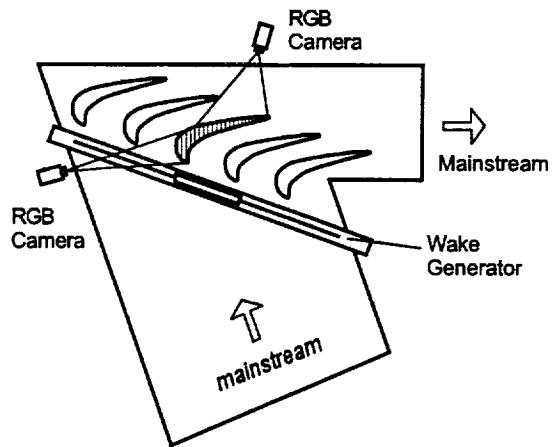
Fig. 1 (a) Five blade cascade with center blade coated
with liquid crystal and viewed by two cameras
(b) A 2-D view of the film-cooled blade model

34
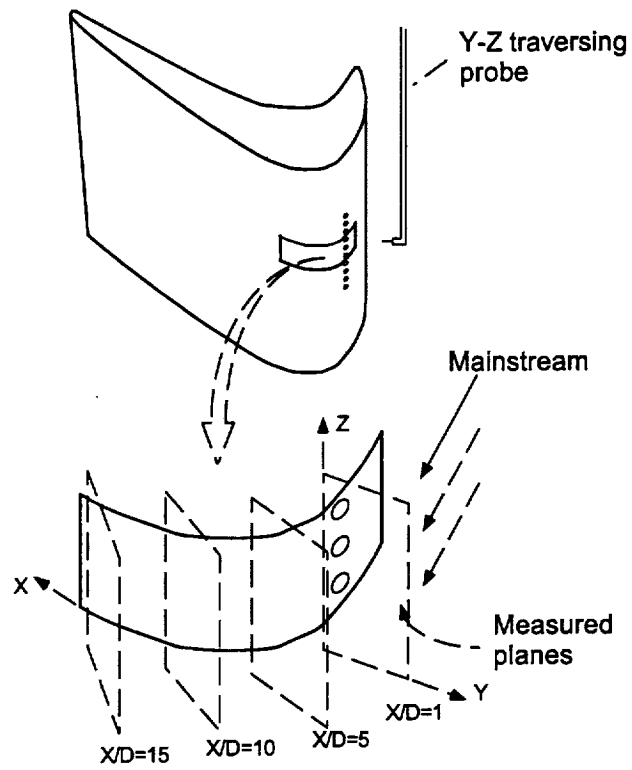
Fig. 2 Measurement planes at selected
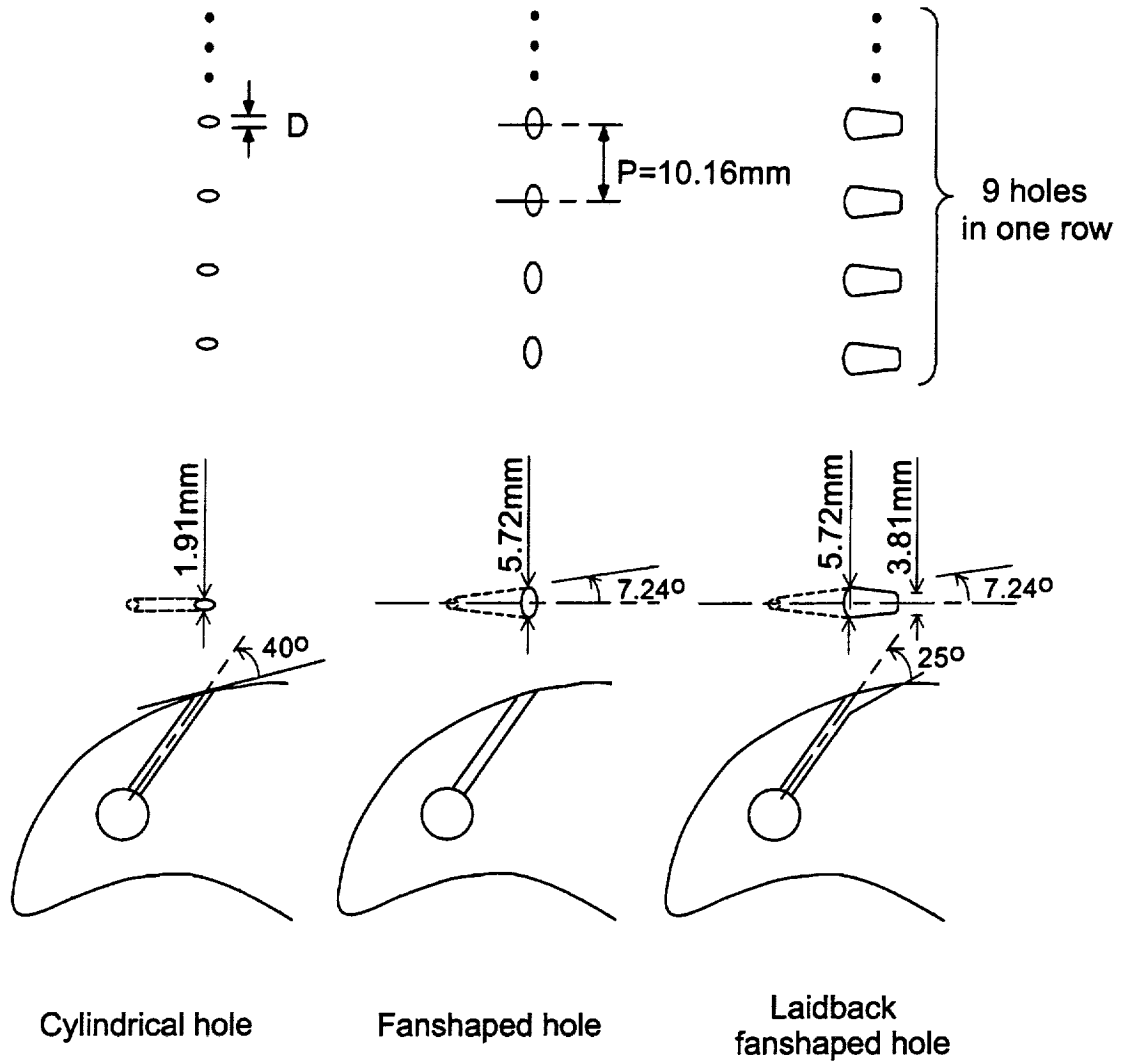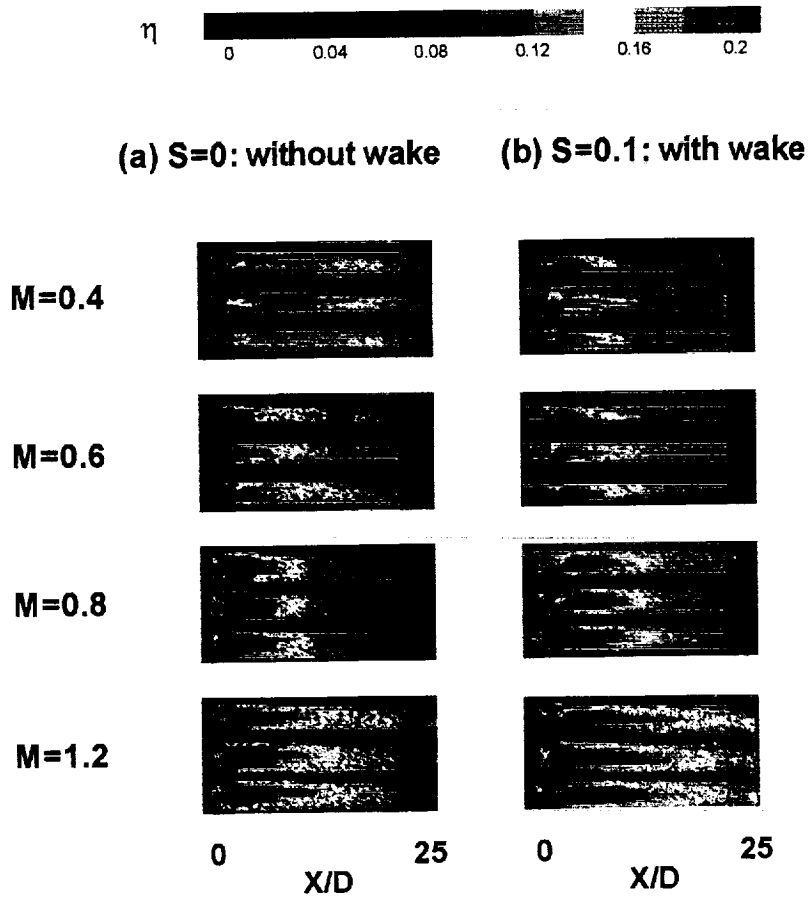locations with a cold-wire probe

P=10.16mm

9 holes
in one row

1.91mm   5.72mm   5.72mm   3.81mm

40°   7.24°   7.24°   25°

Cylindrical hole   Fanshaped hole   Laidback
fanshaped hole

Fig. 3 Film cooling hole geometries

η
0   0.04   0.08   0.12   0.16   0.2

(a) S=0: without wake   **(b) S=0.1: with wake**

M=0.4

M=0.6

M=0.8

M=1.2

0   25   0   25
  X/D   X/D

Fig. 4: Detailed film effectiveness distributions of fanshaped holes
for cases at different blowing ratios, with and without wake effect

37

η scale: 0   0.04   0.08   0.12   0.16   0.2

(a) S=0: without wake   **(b) S=0.1: with wake**

M=0.4

M=0.6

M=0.8

M=1.2

0   **X/D**   25   0   **X/D**   25
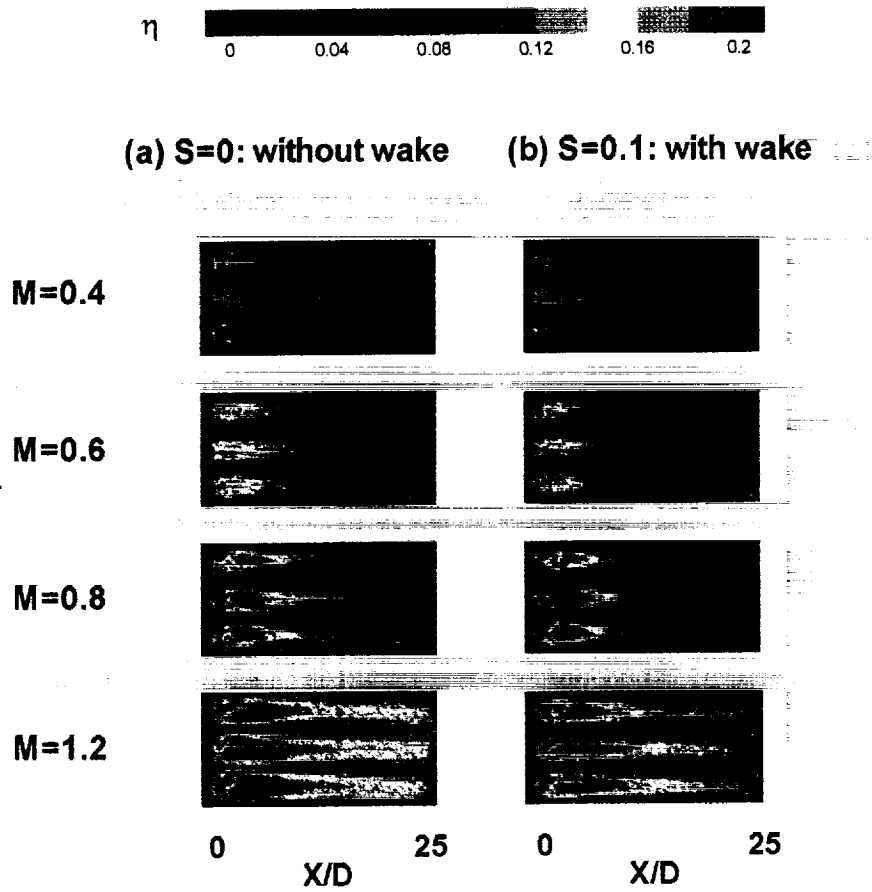
Fig. 5: Detailed film effectiveness distributions of laidback fanshaped holes for cases at different blowing ratios, with and without wake effect
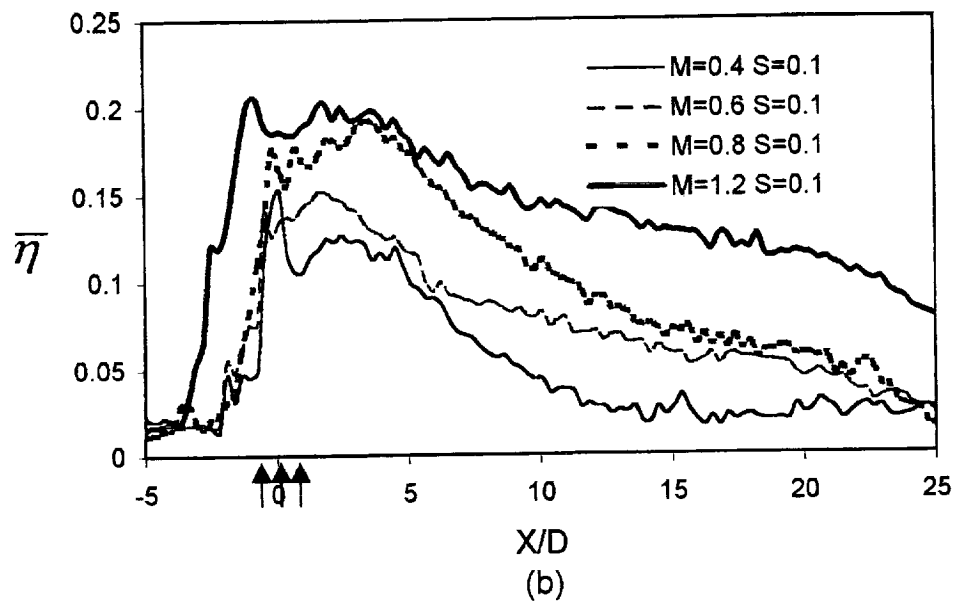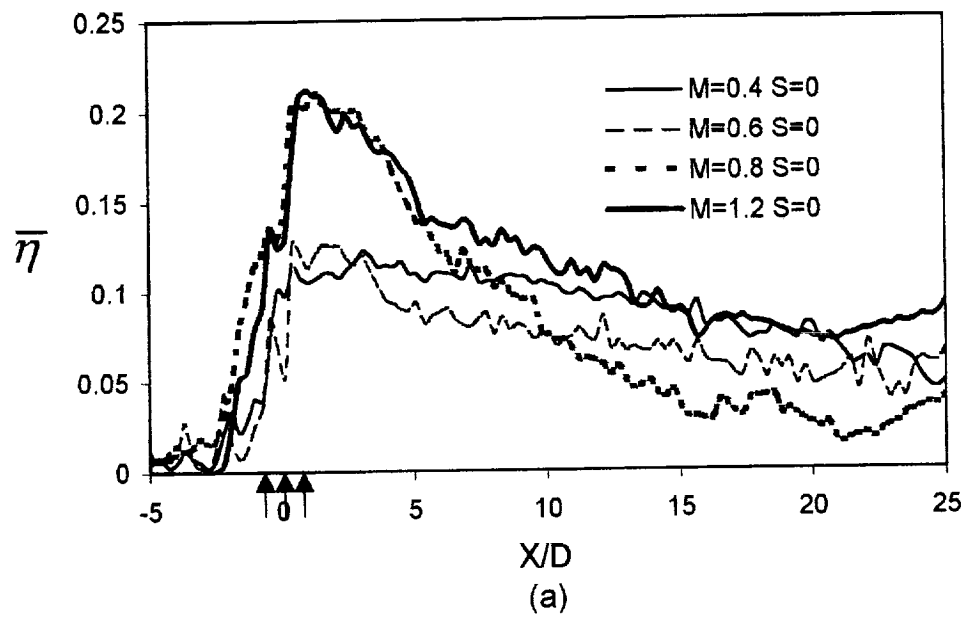
Fig. 6 Spanwise-averaged film effectiveness distribution of fanshaped holes for (a) steady flow, (b) unsteady flow with wake effect
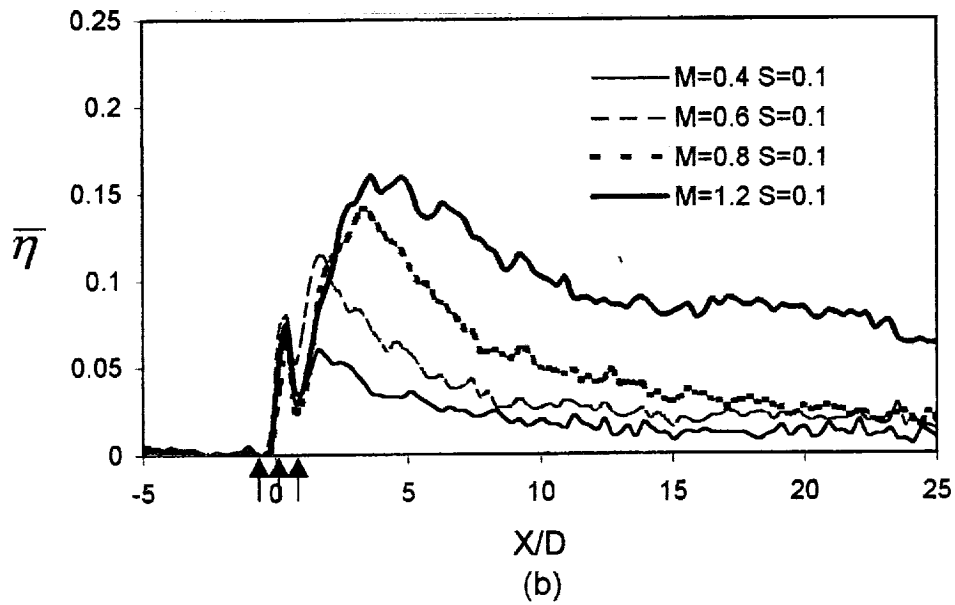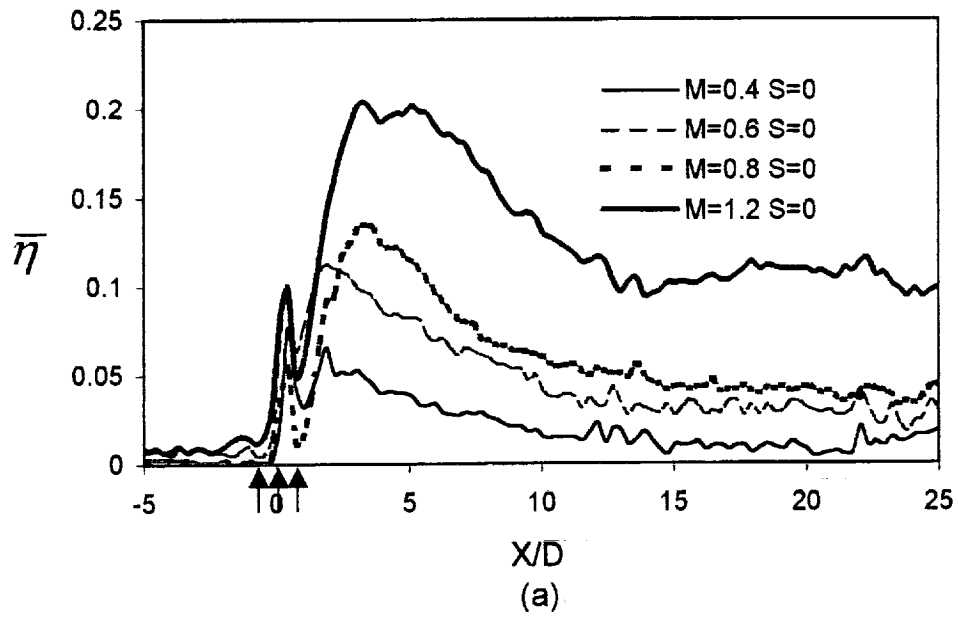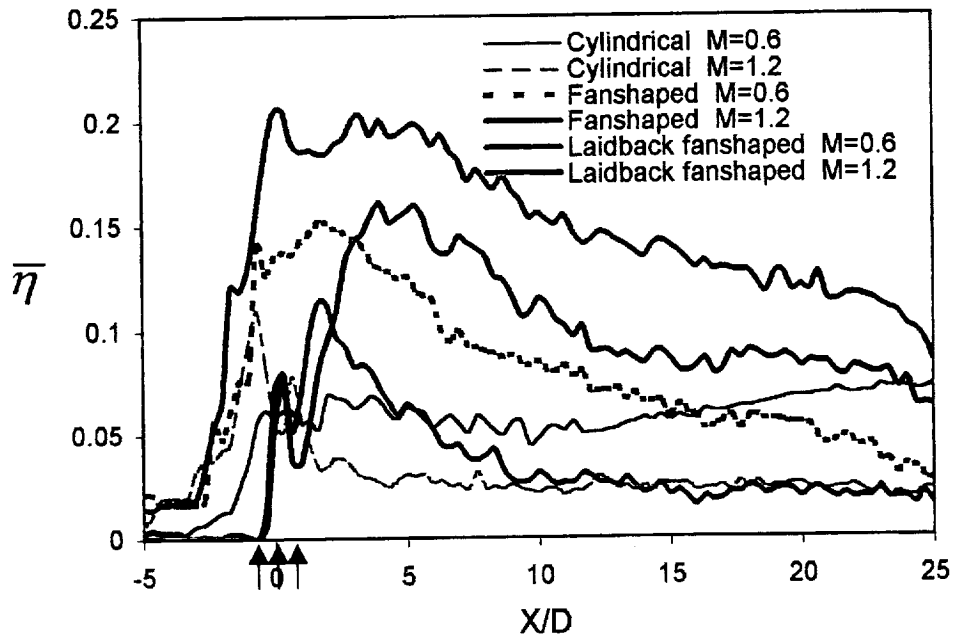
Fig. 7 Spanwise-averaged film effectiveness distribution of Laidback fanshaped holes for (a) steady flow, (b) unsteady flow with wake effect
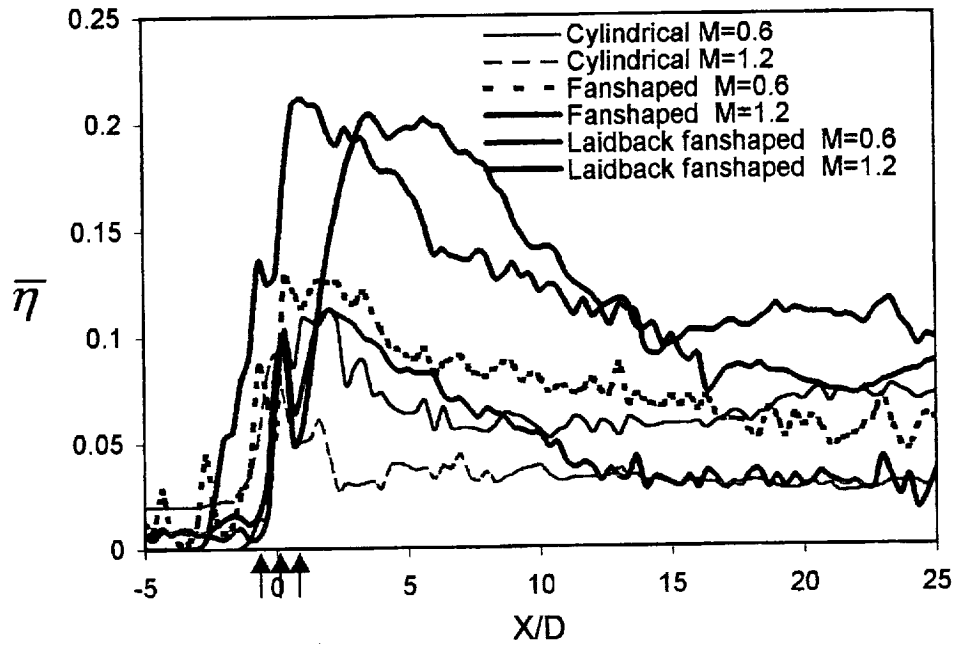
(a) Without wake effect (S=0)

(b) Unsteady flow with wake effect (S=0.1)

Fig. 8 Effect of hole shape on spanwise-averaged film effectiveness
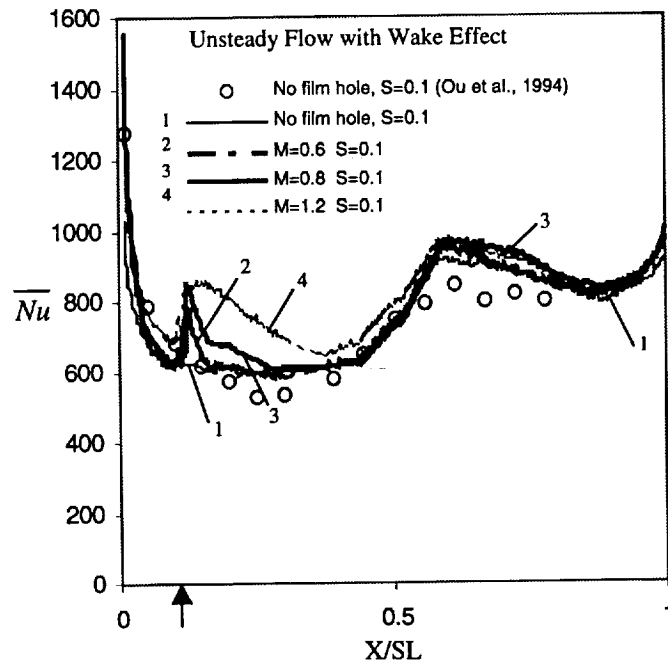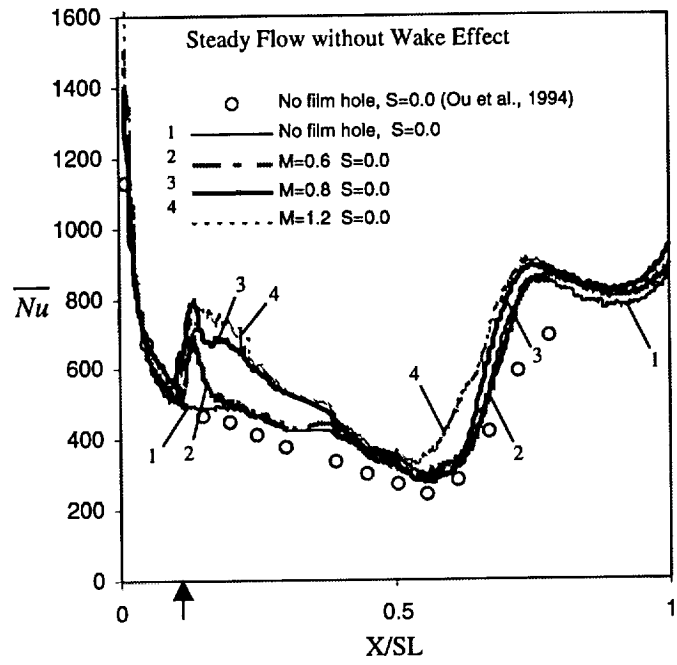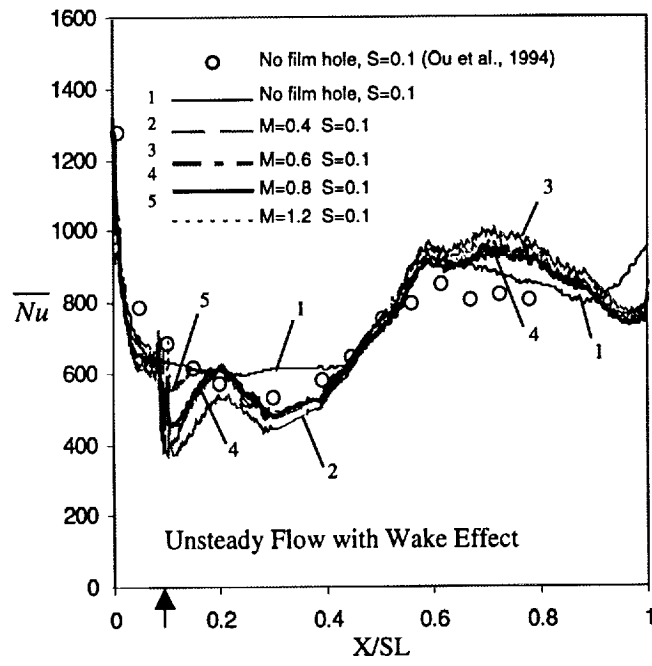distribution for (a) steady flow, (b) unsteady flow with wake effect

Nu

0   200   400   600   800   1000

(a1)

(a2)

(a3)

(a4)

0   X/SL   1

(a) S=0.0, no film hole and M=0.6, 0.8, 1.2

(b1)

(b2)

(b3)

(b4)

0   X/SL   1

(b) S=0.1, no film hole and M=0.6, 0.8, 1.2

Fig. 9: Detailed Nusselt number distributions of cylindrical holes
for cases at different blowing ratios, with and without wake effect

(a) S=0.0, No film holes and M=0.4, 0.6, 0.8, 1.2

(b) S=0.1, No film holes and M=0.4, 0.6, 0.8, 1.2

Fig. 10: Detailed Nusselt number distributions of fanshaped holes for cases at different blowing ratios, and with and without wake effect

Nu 0 200 400 600 800 1000

(a1)

(a2)

(a3)

(a4)

(a5)

0 X/SL 1

(a) S=0.0, No film holes and M=0.4, 0.6, 0.8, 1.2

(b1)

(b2)

(b3)

(b4)

(b5)

0 X/SL 1

(b) S=0.1, No film holes and M=0.4, 0.6, 0.8, 1.2

Fig. 11: Detailed Nusselt number distributions of laidback fanshaped holes for cases at different blowing ratios, and with and without wake effect

44

Fig. 12 Spanwise-averaged Nusselt number distribution of cylindrical holes for (a) steady flow (b) unsteady flow with wake effect

45
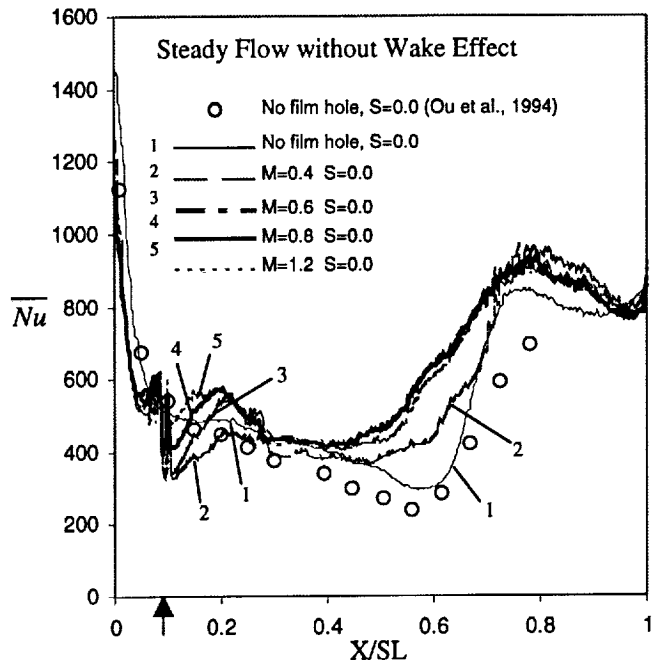
Fig. 13 Spanwise-averaged Nusselt number
distributions of fanshaped holes for (a) steady
flow, (b) unsteady flow with wake effect
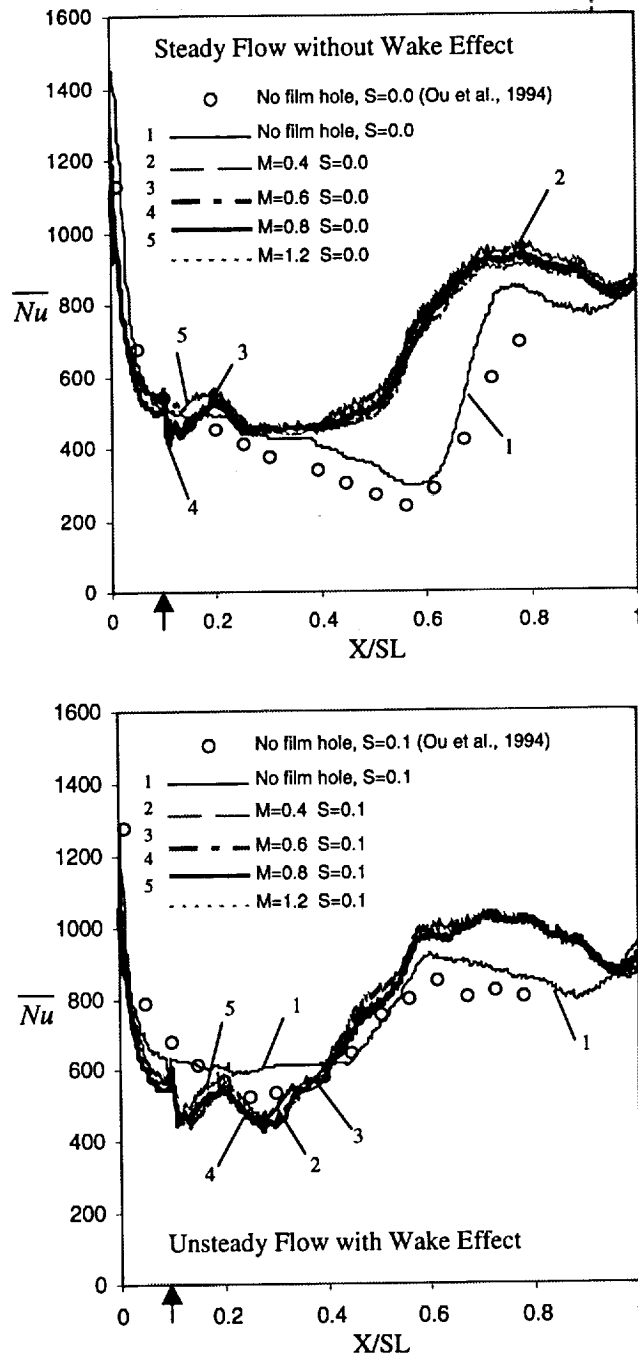
Fig. 14   Spanwise-averaged Nusselt number
distributions of laidback fanshaped holes for (a)
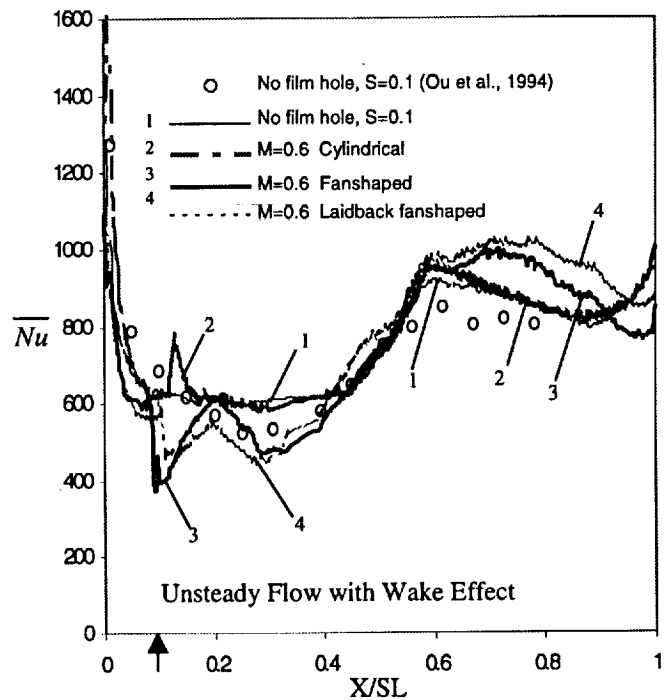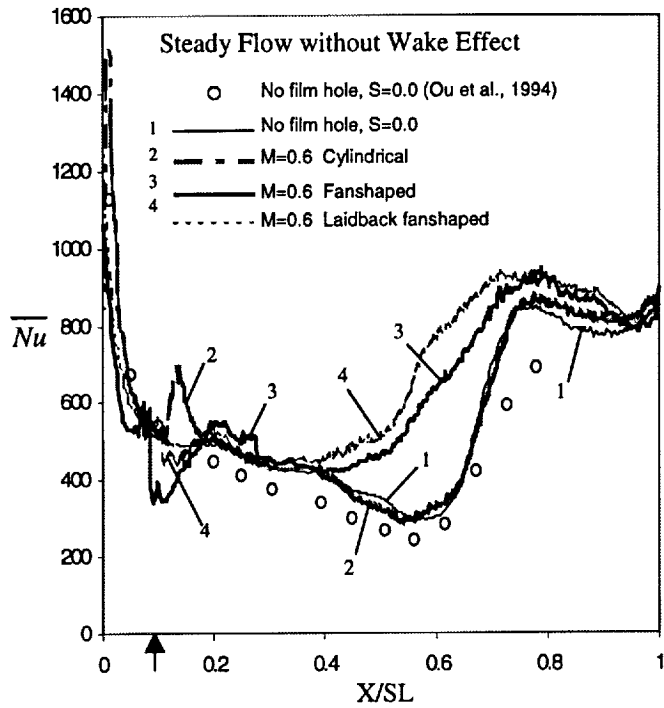steady flow, (b) unsteady flow with wake effect

47

Fig. 15 Effect of hole shape on spanwise-averaged Nusselt number distributions for M=0.6 (a) steady flow, S=0.0, (b) unsteady flow with wake effect, S=0.1
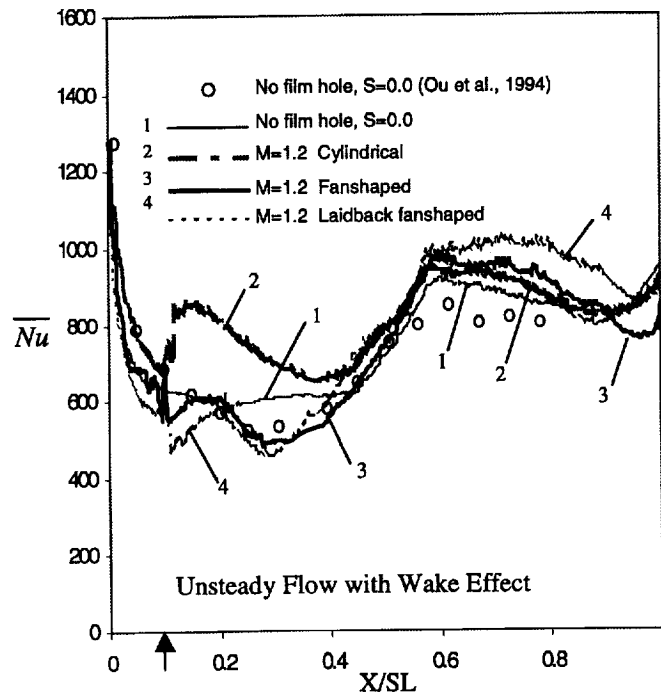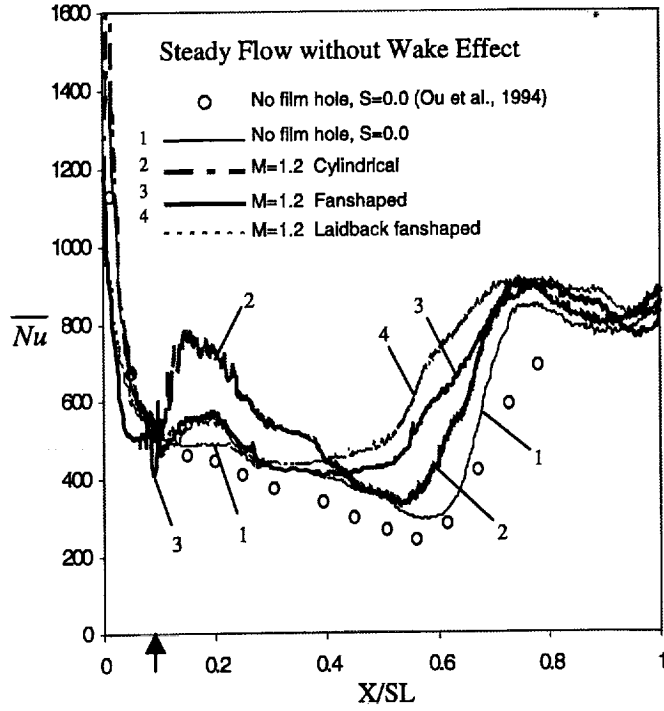
48

Fig. 16 Effect of hole shape on spanwise-averaged
Nusselt number distributions for M=1.2 (a) steady flow,
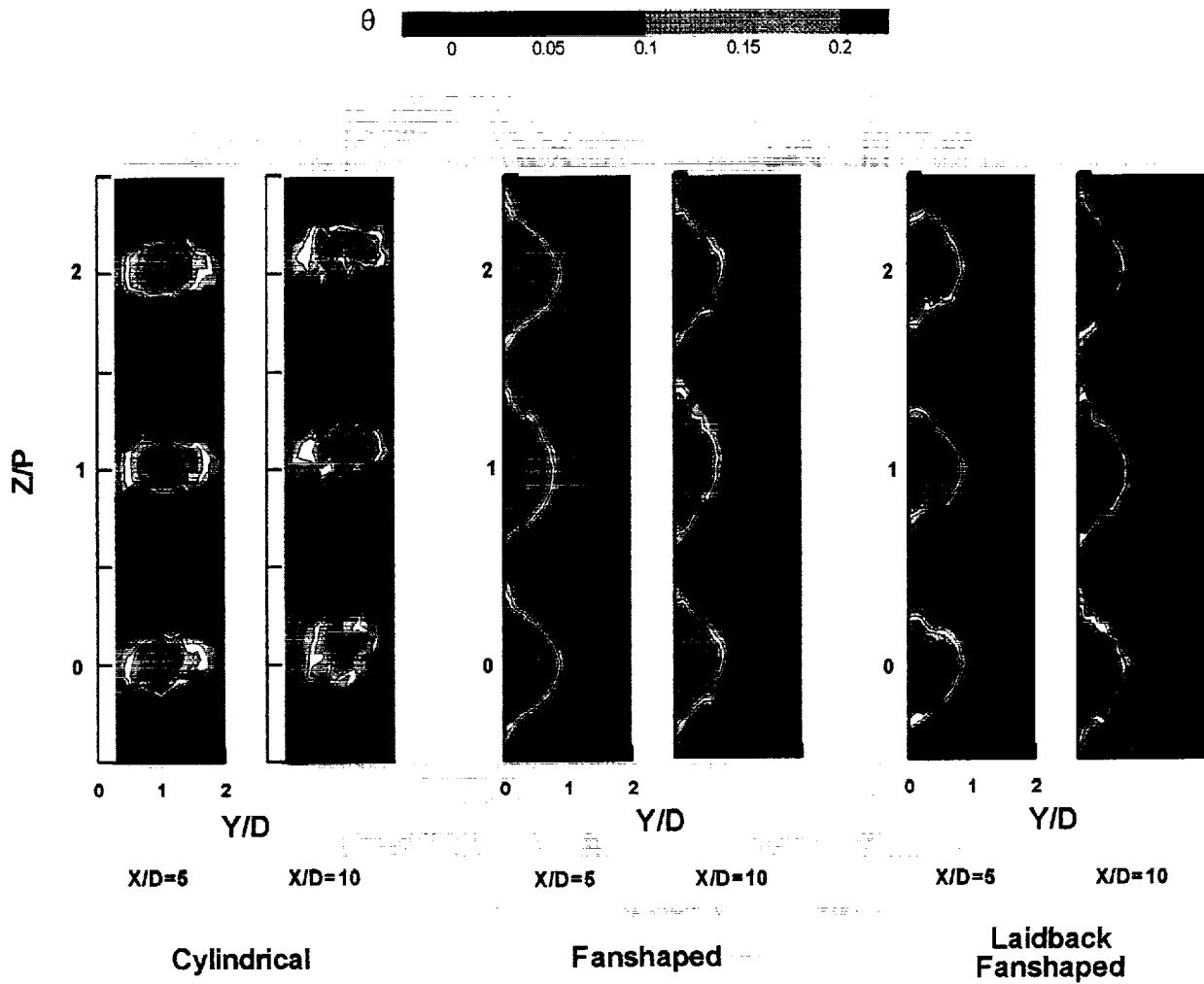S=0.0, (b) unsteady flow with wake effect, S=0.1

49

Fig. 17 The film temperature field at selected locations for the cylindrical,
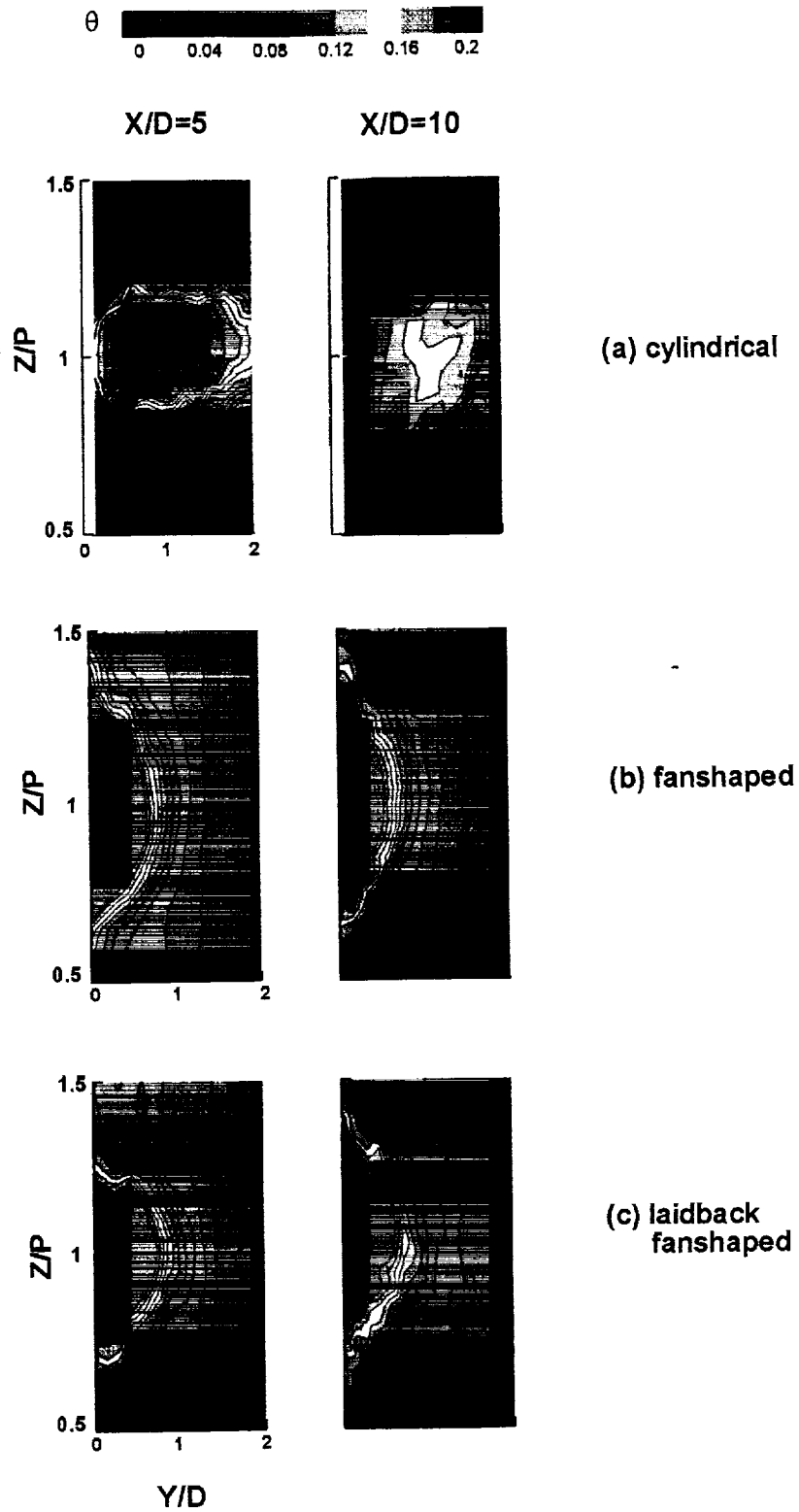fanshaped, and laidback fanshaped holes without wake effect (S=0) at M=1.2

θ

0   0.04 0.08 0.12   0.16 0.2

X/D=5   X/D=10

1.5

Z/P 1   (a) cylindrical

0.5
    0   1   2

1.5

Z/P 1   (b) fanshaped

0.5
    0   1   2

1.5

Z/P 1   (c) laidback
                                              fanshaped

0.5
    0   1   2

Y/D

Fig. 18 Effect of hole shape on detailed film
temperature field for steady flow (S=0) at M=1.2

51

θ   0   0.04   0.08   0.12   0.16   0.2

X/D=5   X/D=10
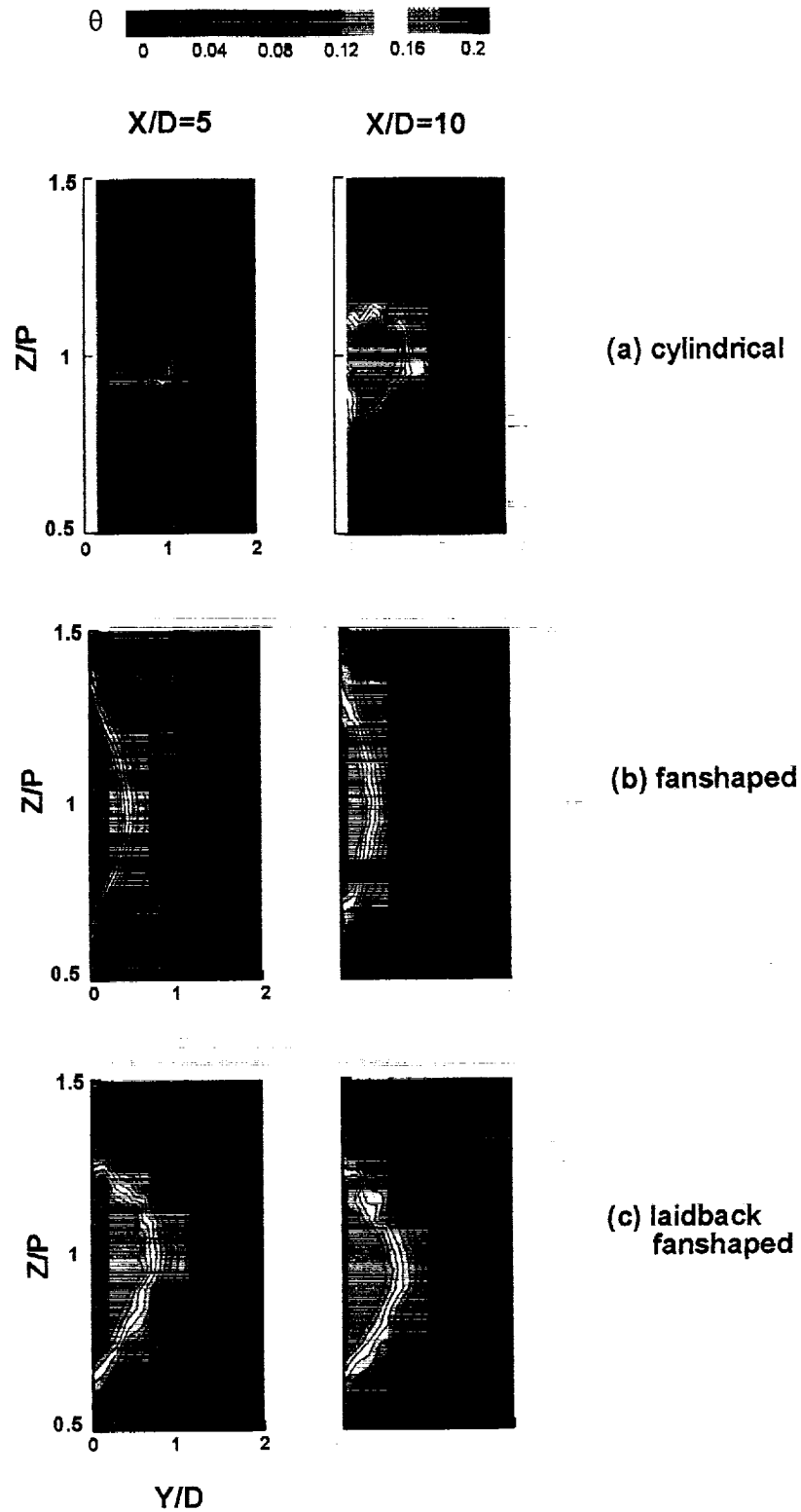
(a) cylindrical

(b) fanshaped

(c) laidback
fanshaped

Y/D

Fig. 19 Effect of hole shape on detailed film
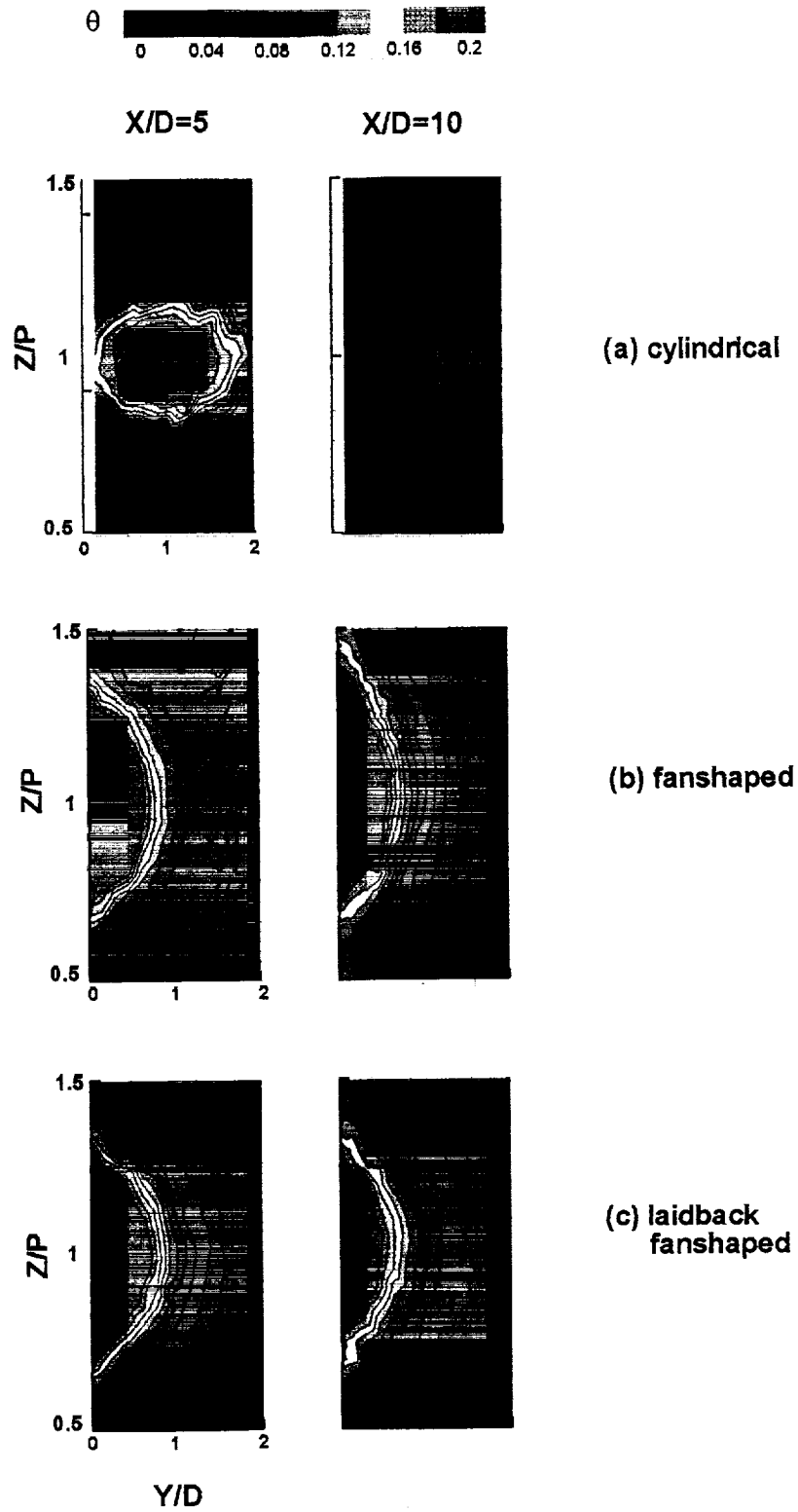temperature field for steady flow (S=0) at M=0.8

Fig. 20 Effect of hole shape on detailed film
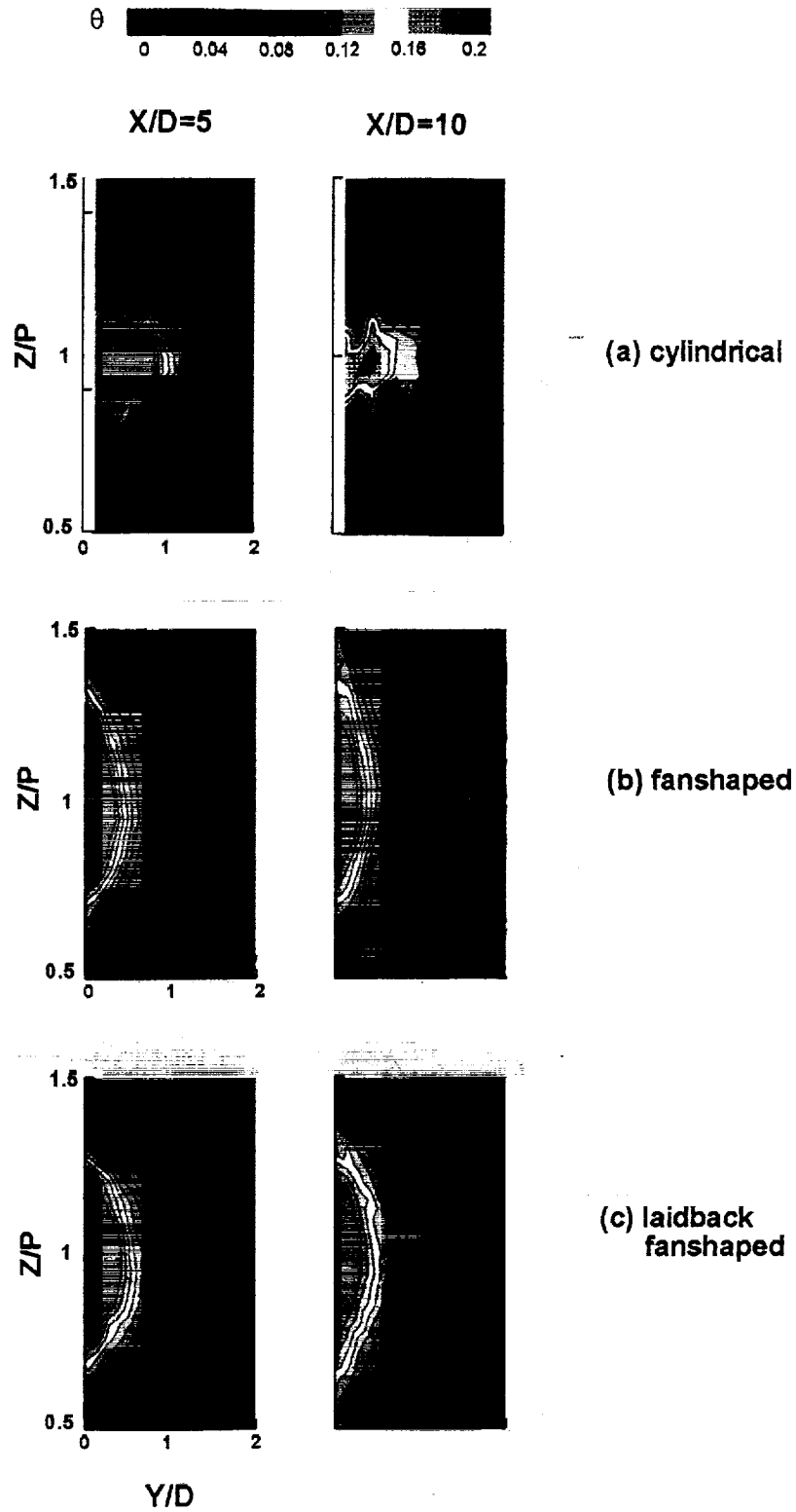temperature field for unsteady flow (S=0.1) at M=1.2

Fig. 21 Effect of hole shape on detailed film
temperature field for unsteady flow (S=0.1) at M=0.8

REPORT DOCUMENTATION PAGE

Public reporting burden for this collection of information is estimated to average 1 hour per response, including the time for reviewing instructions, searching existing data sources, gathering and maintaining the data needed, and completing and reviewing the collection of information. Send comments regarding this burden estimate or any other aspect of this collection of information, including suggestions for reducing this burden, to Washington Headquarters Services, Directorate for Information Operations and Reports, 1215 Jefferson Davis Highway, Suite 1204, Arlington, VA 22202-4302, and to the Office of Management and Budget, Paperwork Reduction Project (0704-0188), Washington, DC 20503.

1. AGENCY USE ONLY (Leave blank)	2. REPORT DATE February 2000	3. REPORT TYPE AND DATES COVERED Final Contractor Report

4. TITLE AND SUBTITLE

Effect of Film-Hole Shape on Turbine Blade Film Cooling Performance

5. FUNDING NUMBERS

WU–714–01–4A–00
NAG3–1656

6. AUTHOR(S)

J.C. Han and S. Teng

7. PERFORMING ORGANIZATION NAME(S) AND ADDRESS(ES)

Texas A&M University
Department of Mechanical Engineering
College Station, Texas 77843–3123

8. PERFORMING ORGANIZATION REPORT NUMBER

E–12176

9. SPONSORING/MONITORING AGENCY NAME(S) AND ADDRESS(ES)

National Aeronautics and Space Administration
John H. Glenn Research Center at Lewis Field
Cleveland, Ohio 44135–3191

10. SPONSORING/MONITORING AGENCY REPORT NUMBER

NASA CR—2000-209932

11. SUPPLEMENTARY NOTES

Project Manager, Philip Poinsatte, Turbomachinery and Propulsion Systems Division, NASA Glenn Research Center, organization code 5820, (216) 433–5898.

12a. DISTRIBUTION/AVAILABILITY STATEMENT

Unclassified - Unlimited
Subject Categories: 02, 07, and 34   Distribution: Nonstandard

This publication is available from the NASA Center for AeroSpace Information, (301) 621–0390.

12b. DISTRIBUTION CODE

13. ABSTRACT (Maximum 200 words)

The detailed heat transfer coefficient and film cooling effectiveness distributions as well as the detailed coolant jet temperature profiles on the suction side of a gas turbine blade were measured using a transient liquid crystal image method and a traversing cold wire and a traversing thermocouple probe, respectively. The blade has only one row of film holes near the gill hole portion on the suction side of the blade. The hole geometries studied include standard cylindrical holes and holes with diffuser shaped exit portion (i.e. fanshaped holes and laidback fanshaped holes). Tests were performed on a five-blade linear cascade in a low-speed wind tunnel. The mainstream Reynolds number based on cascade exit velocity was 5.3×10^5. Upstream unsteady wakes were simulated using a spoke-wheel type wake generator. The wake Strouhal number was kept at 0 or 0.1. Coolant blowing ratio was varied from 0.4 to 1.2. Results show that both expanded holes have significantly improved thermal protection over the surface downstream of the ejection location, particularly at high blowing ratios. However, the expanded hole injections induce earlier boundary layer transition to turbulence and enhance heat transfer coefficients at the latter part of the blade suction surface. In general, the unsteady wake tends to reduce film cooling effectiveness.

14. SUBJECT TERMS

Film cooling; Turbomachinery; Gas turbine; Heat transfer; Heat transfer coefficient; Turbulent heat transfer

15. NUMBER OF PAGES
63

16. PRICE CODE
A04

17. SECURITY CLASSIFICATION OF REPORT	18. SECURITY CLASSIFICATION OF THIS PAGE	19. SECURITY CLASSIFICATION OF ABSTRACT	20. LIMITATION OF ABSTRACT
Unclassified	Unclassified	Unclassified	